AGU Advances

RESEARCH ARTICLE
10.1029/2024AV001241

Peer Review The peer review history for this article is available as a PDF in the Supporting Information.

Key Points:

- The Perseverance rover has collected seven cores of aqueously deposited sandstones and siltstones at the front of Jezero's western fan
- Hydrated sulfate, clay and carbonate minerals in the cores record the history of Mars's volatiles and surface habitability
- The same minerals may preserve organic and inorganic signals of abiotic, prebiotic and biological processes

Supporting Information:

Supporting Information may be found in the online version of this article.

Correspondence to:

T. Bosak and D. L. Shuster,
tbosak@mit.edu;
dshuster@berkeley.edu

Citation:

Bosak, T., Shuster, D. L., Scheller, E. L., Siljeström, S., Zawaski, M. J., Mandon, L., et al. (2024). Astrobiological potential of rocks acquired by the Perseverance rover at a sedimentary fan front in Jezero crater, Mars. *AGU Advances*, *5*, e2024AV001241. https://doi.org/10.1029/2024AV001241

Received 11 MAR 2024
Accepted 31 MAY 2024

Author Contributions:

Conceptualization: T. Bosak, D. L. Shuster, K. A. Farley, E. M. Hausrath
Data curation: E. L. Scheller, S. Siljeström, E. N. Mansbach, A. H. Treiman, J. F. Bell III, S. Bernard

Astrobiological Potential of Rocks Acquired by the Perseverance Rover at a Sedimentary Fan Front in Jezero Crater, Mars

T. Bosak[1], D. L. Shuster[2], E. L. Scheller[1], S. Siljeström[3], M. J. Zawaski[4], L. Mandon[5], J. I. Simon[6], B. P. Weiss[1], K. M. Stack[7], E. N. Mansbach[1], A. H. Treiman[8], K. C. Benison[9], A. J. Brown[10], A. D. Czaja[11], K. A. Farley[5], E. M. Hausrath[12], K. Hickman-Lewis[13,14], C. D. K. Herd[15], J. R. Johnson[16], L. E. Mayhew[17], M. E. Minitti[18], K. H. Williford[19], B. V. Wogsland[20], M.-P. Zorzano[21], A. C. Allwood[7], H. E. F. Amundsen[22], J. F. Bell III[23], K. Benzerara[24], S. Bernard[24], O. Beyssac[24], D. K. Buckner[25], M. Cable[7], F. Calef III[7], G. Caravaca[26], D. C. Catling[27], E. Clavé[28], E. Cloutis[29], B. A. Cohen[30], A. Cousin[26], E. Dehouck[31], A. G. Fairén[21,32], D. T. Flannery[33], T. Fornaro[34], O. Forni[26], T. Fouchet[35], E. Gibbons[36], F. Gomez Gomez[21], S. Gupta[37], K. P. Hand[7], J. A. Hurowitz[38], H. Kalucha[5], D. A. K. Pedersen[39], G. Lopes-Reyes[40], J. N. Maki[7], S. Maurice[26], J. I. Nuñez[16], N. Randazzo[15], J. W. Rice Jr.[23], C. Royer[41], M. A. Sephton[37], S. Sharma[7], A. Steele[42], C. D. Tate[32], K. Uckert[7], A. Udry[12], R. C. Wiens[41], and A. Williams[25]

[1]Department of Earth, Atmospheric and Planetary Sciences, Massachusetts Institute of Technology, Cambridge, MA, USA, [2]Department of Earth and Planetary Science, University of California, Berkeley, CA, USA, [3]RISE Research Institutes of Sweden, Stockholm, Sweden, [4]Department of Geology & Geophysics, Texas A&M University, College Station, TX, USA, [5]Division of Geological and Planetary Sciences, California Institute of Technology, Pasadena, CA, USA, [6]Center for Isotope Cosmochemistry and Geochronology, NASA Johnson Space Center, Houston, TX, USA, [7]Jet Propulsion Laboratory, California Institute of Technology, Pasadena, CA, USA, [8]Lunar and Planetary Institute (USRA), Houston, TX, USA, [9]Department of Geology and Geography, West Virginia University, Morgantown, WV, USA, [10]Plancius Research, Severna Park, MD, USA, [11]Department of Geosciences, University of Cincinnati, Cincinnati, OH, USA, [12]Department of Geosciences, University of Nevada, Las Vegas, NV, USA, [13]The Natural History Museum, London, UK, [14]Dipartimento BiGeA, Università di Bologna, Bologna, Italy, [15]Department of Earth and Atmospheric Sciences, University of Alberta, Edmonton, AB, Canada, [16]Johns Hopkins University, Applied Physics Laboratory, Laurel, MD, USA, [17]Department of Geological Sciences, University of Colorado Boulder, Boulder, CO, USA, [18]Framework, Silver Spring, MD, USA, [19]Blue Marble Space Institute of Science, Seattle, WA, USA, [20]Department of Earth and Planetary Sciences, University of Tennessee, Knoxville, TN, USA, [21]Centro de Astrobiologia (CAB), CSIC-INTA, Madrid, Spain, [22]Center for Space Sensors and Systems, University of Oslo, Kjeller, Norway, [23]Arizona State University, Tempe, AZ, USA, [24]Institut de Minéralogie, de Physique des Matériaux et de Cosmochimie, CNRS UMR 7590, Sorbonne Université, Muséum National d'Histoire Naturelle, Paris, France, [25]Department of Geological Sciences, University of Florida, Gainesville, FL, USA, [26]Institut de Recherche en Astrophysique et Planétologie, Université de Toulouse, CNRS, CNES, Tolouse, France, [27]Department of Earth and Space Sciences, University of Washington, Seattle, WA, USA, [28]DLR - Institute of Optical Sensor Systems, Berlin, Germany, [29]University of Winnipeg, Winnipeg, MB, Canada, [30]NASA Goddard Space Flight Center, Greenbelt, MD, USA, [31]Universite Claude Bernard Lyon1, LGL-TPE, UMR 5276, CNRS, ENSL, UJM, Villeurbanne, France, [32]Department of Astronomy, Cornell University, Ithaca, NY, USA, [33]Queensland University of Technology, Brisbane, QLD, Australia, [34]INAF-Astrophysical Observatory of Arcetri, Florence, Italy, [35]LESIA, Observatoire de Paris, Université PSL, CNRS, Sorbonne Université, Université de Paris, Meudon, France, [36]McGill University, Montreal, QC, Canada, [37]Department of Earth Science and Engineering, Imperial College London, London, UK, [38]Department of Geosciences, Stony Brook University, Stony Brook, NY, USA, [39]Department of Measurement and Instrumentation, Technical University of Denmark, DTU Space, Kongens Lyngby, Denmark, [40]Research Group ERICA, Universidad de Valladolid, Valladolid, Spain, [41]Earth, Atmospheric, and Planetary Sciences, Purdue University, West Lafayette, IN, USA, [42]Earth and Planetary Laboratory, Carnegie Institution for Science, Washington, DC, USA

Abstract The Perseverance rover has collected seven oriented samples of sedimentary rocks, all likely older than the oldest signs of widespread life on Earth, at the exposed base of the western fan in Jezero crater, Mars. The samples include a sulfate- and clay-bearing mudstone and sandstone, a fluvial sandstone from a stratigraphically low position at the fan front, and a carbonate-bearing sandstone deposited above the sulfate-bearing strata. All samples contain aqueously precipitated materials and most or all were aqueously deposited. Although the rover instruments have not confidently detected organic matter in the rocks from the fan front, the much more sensitive terrestrial instruments will still be able to search for remnants of prebiotic chemistries and

Formal analysis: T. Bosak, D. L. Shuster, E. L. Scheller, S. Siljeström, M. J. Zawaski, L. Mandon, J. I. Simon, B. P. Weiss, K. M. Stack, E. N. Mansbach, A. H. Treiman, K. C. Benison, A. J. Brown, A. D. Czaja, K. A. Farley, E. M. Hausrath, K. Hickman-Lewis, J. R. Johnson, L. E. Mayhew, M. E. Minitti, K. H. Williford, B. V. Wogsland, M.-P. Zorzano, K. Benzerara, S. Bernard, O. Beyssac, D. K. Buckner, M. Cable, F. Calef III, G. Caravaca, D. C. Catling, E. Clavé, E. Cloutis, B. A. Cohen, A. Cousin, E. Dehouck, A. G. Fairén, D. T. Flannery, T. Fornaro, O. Forni, T. Fouchet, E. Gibbons, F. Gomez Gomez, S. Gupta, K. P. Hand, H. Kalucha, D. A. K. Pedersen, G. Lopes-Reyes, J. N. Maki, S. Maurice, J. I. Nuñez, N. Randazzo, J. W. Rice Jr., C. Royer, S. Sharma, A. Steele, C. D. Tate, A. Udry, R. C. Wiens

Funding acquisition: T. Bosak, D. L. Shuster, S. Siljeström, M. J. Zawaski, J. I. Simon, B. P. Weiss, K. M. Stack, A. H. Treiman, K. C. Benison, A. J. Brown, A. D. Czaja, K. A. Farley, E. M. Hausrath, K. Hickman-Lewis, C. D. K. Herd, J. R. Johnson, L. E. Mayhew, M. E. Minitti, M.-P. Zorzano, A. C. Allwood, B. A. Cohen, E. Dehouck, A. Udry

Investigation: T. Bosak, D. L. Shuster, E. L. Scheller, S. Siljeström, M. J. Zawaski, L. Mandon, J. I. Simon, B. P. Weiss, K. M. Stack, E. N. Mansbach, A. H. Treiman, K. C. Benison, A. J. Brown, A. D. Czaja, K. A. Farley, E. M. Hausrath, K. Hickman-Lewis, C. D. K. Herd, J. R. Johnson, L. E. Mayhew, M. E. Minitti, K. H. Williford, B. V. Wogsland, M.-P. Zorzano, A. C. Allwood, H. E. F. Amundsen, J. F. Bell III, K. Benzerara, S. Bernard, O. Beyssac, D. K. Buckner, M. Cable, F. Calef III, G. Caravaca, D. C. Catling, E. Clavé, E. Cloutis, B. A. Cohen, A. Cousin, E. Dehouck, A. G. Fairén, D. T. Flannery, T. Fornaro, O. Forni, T. Fouchet, E. Gibbons, F. Gomez Gomez, S. Gupta, K. P. Hand, J. A. Hurowitz, H. Kalucha, D. A. K. Pedersen, G. Lopes-Reyes, J. N. Maki, S. Maurice, J. I. Nuñez, N. Randazzo, J. W. Rice Jr., C. Royer, M. A. Sephton, S. Sharma, A. Steele, C. D. Tate, K. Uckert, A. Udry, R. C. Wiens, A. Williams

Methodology: T. Bosak, J. I. Simon, B. P. Weiss, K. M. Stack, E. N. Mansbach, A. H. Treiman, A. C. Allwood, J. F. Bell III, K. Benzerara, S. Bernard, O. Beyssac, M. Cable, F. Calef III, G. Caravaca, D. C. Catling, A. Cousin, A. G. Fairén, O. Forni, E. Gibbons, S. Gupta, K. P. Hand, J. A. Hurowitz, H. Kalucha, D. A. K. Pedersen, J. N. Maki, S. Maurice, J. I. Nuñez, N. Randazzo, K. Uckert, R. C. Wiens

Project administration: K. M. Stack, E. N. Mansbach, K. A. Farley, E. M. Hausrath

past life, and study Mars's past habitability in the samples returned to Earth. The hydrated, sulfate-bearing mudstone has the highest potential to preserve organic matter and biosignatures, whereas the carbonate-bearing sandstones can be used to constrain when and for how long Jezero crater contained liquid water. Returned sample science analyses of sulfate, carbonate, clay, phosphate and igneous minerals as well as trace metals and volatiles that are present in the samples acquired at the fan front would provide transformative insights into past habitable environments on Mars, the evolution of its magnetic field, atmosphere and climate and the past and present cycling of atmospheric and crustal water, sulfur and carbon.

Plain Language Summary The Perseverance rover collected seven oriented samples of bedrock at the front of the apron-like sediment deposit in the western side of Jezero crater, Mars. Grains and cements in these sedimentary rocks were likely deposited by water or formed in the presence of water in a range of past environments that predate the first signs of life on Earth. This study describes the geologic context and chemical composition of these samples and discusses how, upon return to Earth, they can be used to search for potential signs of past life, understand when and for how long Mars was habitable and why its climate changed. Studies of the returned samples would seek to detect and analyze organic compounds that may be present below the detection limit of the rover instruments, particularly in the finest-grained rocks, and look for the traces of prebiotic processes or past life in all collected samples of sedimentary rocks. Additional analyses can also constrain tell us when, why and for how long the rivers and lakes existed in Jezero crater. The presence of diverse materials in rocks that were deposited by or into water can transform current views of Mars science and habitability outside of Earth.

1. Introduction

Jezero crater was selected as the landing site of the Perseverance rover mission because it contains sedimentary rocks that can enable the search for potential signs of early life and prebiotic organic processes on Mars because they are thought to have been aqueously deposited more than 3.5 billion years ago (Farley et al., 2020; Grant et al., 2018; Williford et al., 2018). Past observations by rovers and orbiters motivated many of these efforts by revealing past water-containing, habitable environments on Mars (e.g., Grotzinger et al., 2014; Squyres et al., 2004). However, instruments on rovers cannot provide the combined small-scale isotopic, chemical and textural information required to recognize potential signs of prebiotic processes and early microbial life in martian rocks. Although analyses of various martian meteorites in terrestrial laboratories could, most martian meteorites lack a known geologic context, are igneous and do not sample past environments where life would have thrived, and have been exposed to terrestrial contamination. Thus, the scientific community has prioritized the return of Martian rock samples with known geologic context for at least a decade (Beaty et al., 2019; Farley et al., 2020; National Academies of Sciences, Engineering, and Medicine, 2022; National Research Council, 2011; Williford et al., 2018).

Rocks thought to record past water activity in Jezero crater reside in two fans that extend from two valley network inlet channels, one at the western and the other at the northern side of the crater (Fassett & Head, 2005, 2008). Not only do the older estimates of aqueous activity in these fans (Fassett & Head, 2008, 2011; Goudge et al., 2015; Holm-Alwmark et al., 2021; Mangold et al., 2020; Quantin-Nataf et al., 2023) predate the oldest morphological and chemical evidence for microbial life on Earth at 3.5–3.4 Ga (Allwood et al., 2006; Hickman-Lewis et al., 2019; Sugitani et al., 2013; Tice & Lowe, 2004; Walsh & Lowe, 1999; Westall et al., 2015), but orbital signals of hydration, Fe/Mg-smectite clays (Ehlmann, Mustard, Fassett, et al., 2008; Goudge et al., 2015) and magnesium carbonates in Jezero crater (Ehlmann, Mustard, Murchie, et al., 2008; Goudge et al., 2015; Horgan et al., 2020) indicate the presence of materials that would not survive metamorphic alteration, weathering and extensive post-depositional fluid flow (Bosak et al., 2021). The latter processes have fueled controversial interpretations of the oldest biosignatures in terrestrial rocks (Alleon & Summons, 2019; Allwood et al., 2018; Bernard et al., 2021; Nutman et al., 2016; Rosing, 1999; Zawaski et al., 2020).

Cognizant of the great importance of aqueously deposited sedimentary rocks that likely sample past habitable environments on Mars, the Perseverance rover team designed The Fan Front Campaign to collect a suite of sedimentary rock cores. Here, we describe the campaign, sampling and documentation related to the samples collected by the Perseverance rover at the front of the western sediment fan in Jezero crater (Section 2), and

Resources: T. Bosak, K. M. Stack, E. N. Mansbach, L. E. Mayhew, M. E. Minitti, K. H. Williford, M.-P. Zorzano, A. C. Allwood, J. F. Bell III, M. Cable, G. Caravaca, A. Cousin, A. G. Fairén, S. Gupta, K. P. Hand, J. A. Hurowitz, H. Kalucha, D. A. K. Pedersen, J. N. Maki, S. Maurice, J. I. Nuñez, N. Randazzo, K. Uckert, R. C. Wiens
Software: S. Maurice, N. Randazzo
Supervision: T. Bosak, D. L. Shuster, B. P. Weiss, K. M. Stack, E. N. Mansbach, K. A. Farley, E. M. Hausrath, L. E. Mayhew, M. E. Minitti, A. C. Allwood, H. E. F. Amundsen, J. F. Bell III, S. Bernard, M. Cable, G. Caravaca, A. Cousin, A. G. Fairén, S. Gupta, K. P. Hand, J. A. Hurowitz, H. Kalucha, D. A. K. Pedersen, J. N. Maki, S. Maurice, J. I. Nuñez, N. Randazzo, K. Uckert, R. C. Wiens
Validation: T. Bosak, D. L. Shuster, E. L. Scheller, S. Siljeström, E. Clavé, B. A. Cohen, A. Cousin, A. G. Fairén, O. Forni, E. Gibbons, D. A. K. Pedersen, J. N. Maki, S. Maurice, J. I. Nuñez, N. Randazzo, R. C. Wiens
Visualization: T. Bosak, D. L. Shuster, E. L. Scheller, S. Siljeström, M. J. Zawaski, L. Mandon, J. I. Simon, K. M. Stack, E. N. Mansbach, A. H. Treiman, K. C. Benison, J. R. Johnson, L. E. Mayhew, M. E. Minitti, K. H. Williford, C. D. Tate
Writing – original draft: T. Bosak, D. L. Shuster
Writing – review & editing: T. Bosak, D. L. Shuster, E. L. Scheller, S. Siljeström, M. J. Zawaski, L. Mandon, J. I. Simon, B. P. Weiss, K. M. Stack, E. N. Mansbach, K. C. Benison, A. J. Brown, K. A. Farley, E. M. Hausrath, K. Hickman-Lewis, C. D. K. Herd, J. R. Johnson, S. Bernard, O. Beyssac, D. K. Buckner, M. Cable, E. Clavé, B. A. Cohen, A. G. Fairén, T. Fornaro, T. Fouchet, F. Gomez Gomez, R. C. Wiens

Table 1
Key to Sampled Cores and Associated Abraded Patches

Outcrop (map)	Member	Abrasion	Core for main cache	Core for three forks cache
Amalik	*Amalik*	*Novarupta*	*Mageik*	*Shuyak and WB3*
Hidden Harbor	*Yori Pass*	*Uganik Island*	*Kukaklek*	–
Wildcat Ridge	*Hogwallow Flats*	*Berry Hollow*	*Hazeltop*	*Bearwallow*
Skinner Ridge	*Lower Rockytop*	*Thornton Gap*	*Swift Run and WB2*	*Skyland*

Note. Indicated are Stratigraphic Position (Member) and Placement in the Three Forks Cache or Main Cache.

summarize the textural, mineralogical, and compositional evidence for their aqueous deposition and alteration (Section 3). In Section 4, we discuss the potential of these samples to, upon return to Earth, enable the search for potential biosignatures and investigations of Martian volatiles and changing habitability within an established stratigraphic and temporal context.

2. Campaign, Sampling and Documentation

2.1. Planning and Methodology for Sampling During the Fan Front Campaign

After exploring the igneous crater floor (e.g., Farley et al., 2022) and collecting samples of aqueously altered igneous rocks (Simon et al., 2023), the planning process for the Fan Front Campaign was conducted in early 2022 using orbital imagery and spectroscopy (Stack et al., 2020). This process identified four paired samples to be collected at the front of the western Jezero fan: (a and b) two different samples of lacustrine sediments with the potential for biosignature preservation; (c) one relatively coarse-grained sedimentary sample for constraining the geochronology of fan deposition and Jezero catchment provenance studies; and (d) one regolith sample. This sampling plan addressed some of the many objectives of the iMOST report (Beaty et al., 2019), focusing on the samples that represented the geologic diversity of this area, while having the capacity to preserve organic compounds, chemical or morphological signals of past habitable conditions and potential biosignatures.

2.2. STOP List and Sample Documentation

Before acquiring each core, the rover drill used an Abrading Bit to expose a fresh, 5–10 mm deep, circular interior region of the nearby outcrop, called an abraded patch, for analysis (Moeller et al., 2021). Table 1 presents the names of these abrasion patches and relates them to the names of the outcrops and samples.

A systematic set of in situ instrument activities, called the Standardized Observation Protocol (STOP) list, accompanies the abrasion and sample collection. The STOP analyses document the geological context and the specific outcrops targeted for sampling and includes images at multiple scales along with chemical and mineralogical analyses of the outcrop surface and abraded patch (see Simon et al., 2023 for details). The outcrop is characterized by Mastcam-Z (workspace context, targeted, and multispectral imaging; Bell et al. (2021)) and SuperCam Remote Micro-Imaging, laser induced breakdown spectroscopy, visible and infrared spectroscopy (VISIR) and Raman spectroscopy (Maurice et al., 2021; Wiens et al., 2021)]. Additional STOP-list analyses of the abraded patches include imaging by a wide-angle camera, Wide Angle Topographic Sensor for Operations and eNgineering (WATSON) (Minitti et al., 2021), detection of minerals and potential organic compounds by ultraviolet (UV) Raman and luminescence spectroscopy using the Scanning Habitable Environments with Raman & Luminescence for Organics & Chemicals (SHERLOC) instrument (Bhartia et al., 2021), and the detection of major elements in the abraded patch by micro (X-ray fluorescence) XRF using the Planetary Instrument for X-ray Lithochemistry (PIXL) instrument (Allwood et al., 2020).

Upon successful sampling, the Science Team processed the instrument data and used the information from the STOP list to write Initial Reports (IRs) for each core within weeks of sample acquisition. The standardized narrative in the IRs summarizes the sample lithologies and compositions, their geologic and stratigraphic context, the rationale for sampling and interpretations that are available at the time of sampling and at the completion of the STOP list activities. The Initial Reports from this and previous campaigns are available publicly and reside in the NASA Planetary Data System (PDS) at https://pds-geosciences.wustl.edu/missions/mars2020/returned_sample_science.htm. All geographic and geological names presented here are informal.

Table 2
Summary of All Cores and Witness Tube Assemblies (Blanks)

Core	Drill sol	Seal sol	Length (mm)	Rock type[a]	Core fracturing	Anomalies
Shuyak	575	575	55.5	Coarse mudstone	ND + small fragment	None
Mageik	579	619	73.6	Coarse mudstone	ND	Sealed 40 sols after drilling
Hazeltop	509	509	59.7	Fine-grained siltstone or coarse mudstone	ND	None
Bearwallow	516	516	62.4	Fine-grained siltstone or coarse mudstone	ND	None
Kukaklek	623	631	49.7	Fine sandstone	ND + small fragment	Sealed 8 days after drilling
Swift Run	490	490	67	Sandstone	ND	None
Skyland	495	495	58.5	Sandstone	ND	None
WB 2	499	499				None
WB 3	584	586				Sealed late, the tube left the sealing station on sol 591

Note. WB: witness blank. ND: not detected. [a]Based on the grain size classification by Lazar et al. (2015) and Wentworth (1922).

2.3. Sampling Process

The Perseverance rover acquired two types of samples during the Fan Front Campaign. First, seven rock samples with diameters of 13 mm and lengths from 49.7 to 73.5 mm (Table 2) were drilled using the rotary percussive coring drill (Moeller et al., 2021). All of these were taken from bedrock so that they can be related to the regional stratigraphic and geologic context and so that their original orientations prior to sampling can be reconstructed. With respect to the latter, all samples were oriented in martian geographic coordinates to better than 2.6° uncertainty (3σ) (Weiss et al., 2024). As in the earlier Crater Floor Campaign (Simon et al., 2023), six of the seven cores were collected as paired samples of three different outcrops; one core from each pair was placed in the Three Forks Cache and one remained on the rover. Second, two unoriented samples of loose regolith were acquired; these are discussed by Hausrath et al. (2023).

2.4. Witness Tubes

In addition to the tubes used for storing the samples, five Witness Tube Assemblies (WTAs) were included on Perseverance's payload (Moeller et al., 2021) as recorders of potential contaminants to which the rock cores might have been exposed from the rover. Four of these "witness tubes" are identical, located in sheaths within the Adaptive Caching Assembly (ACA WTA tubes), protected by fluid mechanical particle barriers and isolated from volatile organic molecules by a tortuous path of gettering surfaces until activation (Moeller et al., 2021). To activate a WTA, the seal is punctured using the volume probe inside the ACA. Thereafter, the WTAs are processed in the same way as the rock cores except there is no contact between drill bit and rock.

Because the largest outgassing from the rover is expected early in the mission, the plan was to process two ACA WTA tubes at the earliest opportunity to do so. Engineering constraints allowed this to occur during the Delta Campaign. The first ACA tube was processed after sampling at *Skinner Ridge* on sol 499. The second ACA was processed directly over the abraded patch *Novarupta* at *Amalik* after sampling of *Shuyak* and *Mageik* (Figure 1; Table 2).

3. Results

Perseverance encountered the first outcrops of sedimentary rocks at a site called *Amalik* on sol 424 (Figure 1; Stack et al., 2024). *Enchanted Lake* contains clastic sedimentary facies consistent with subaqueous deposition (Stack et al., 2024). The rover then explored sections in the laterally-equivalent *Hawksbill Gap* region to identify outcrops suitable for in situ analyses and sampling (Figure 1; Stack et al., 2024).

On sol 477, Perseverance arrived at the *Skinner Ridge* outcrop (Figure 1), where it acquired the *Swift Run* and the *Skyland* cores (Table 1). These two cores fulfilled the desired characteristics for the coarse-grained sediment sample from the fan front that contains a heterogeneous population of detrital materials deposited into the fan,

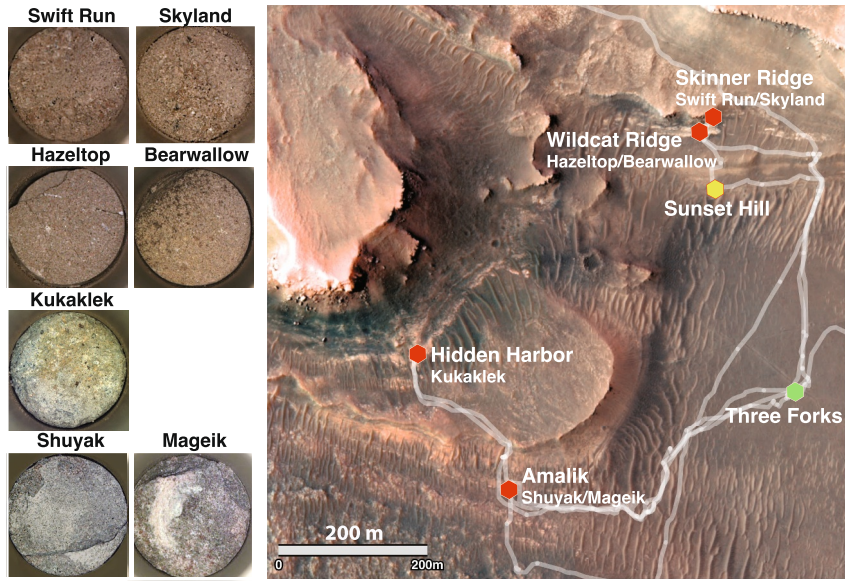

Figure 1. Rock cores acquired during the Fan Front Campaign. CacheCam images of the cores in their container tubes are on the left. Red symbols on the High-Resolution Imaging Experiment (HiRISE) map in the right show the locations of the sampled outcrops and the corresponding cores. *Shuyak* and *Mageik* were sampled at *Amalik* (Figure 2), *Hazeltop* and *Bearwallow* at *Wildcat Ridge* (Figure 3), *Kukaklek* at *Hidden Harbor* (Figure 4) and *Swift Run* and *Skyland* at *Skinner Ridge* (Figure 5). *Sunset Hill* (yellow symbol) was abraded, but the rock collapsed during abrasion, so it was not sampled. All cores are 13 mm in diameter. White lines on the map delineate the rover's trajectory during the Fan Front Campaign. Green symbol shows the location of the Three Forks Cache.

including grains that may have originated outside of Jezero crater, sand-sized or larger grains that enable geochronology, as well as aqueously precipitated minerals such as carbonates and sulfates. Perseverance then processed a WTA (Table 2; Moeller et al., 2021) and drove away toward *Wildcat Ridge* (Figure 1).

Upon arriving at *Wildcat Ridge*, remote-sensing and proximity science observations revealed a fine-grained sedimentary rock at a relatively low stratigraphic position (Table 1; Stack et al., 2024). The rover sampled two cores at this locality: the *Hazeltop* and the *Bearwallow* cores are fine-grained sedimentary rocks that may preserve organic compounds. To increase the number of such samples, the single *Kukaklek* core was collected from *Hidden Harbor* (Figure 1), a lateral equivalent of *Wildcat Ridge* at *Yori Pass* (Table 2). This core was not one of the four samples baselined during campaign planning and was reserved for the main cache on the rover.

Upon return to *Amalik* (Figure 1), the rover acquired the *Shuyak* core and the *Mageik* core. Due to a series of failed attempts to dispense the paired seal for the *Mageik* tube, this core was sealed using a different seal (Table 2). These two cores fulfill the desired characteristics for an aqueously deposited sedimentary rock sample from a low stratigraphic position at the fan front. After the coring of *Mageik*, another WTA was processed at this outcrop (Table 2).

3.1. Stratigraphy and Sedimentology

All samples collected from Jezero fan front have a well-constrained geologic context (Table 1; Stack et al., 2024). The outcrop, bed and grain-size analyses (Tables 2 and 3) support the interpretation of these samples as deposited by water in environments that are interpreted to have transitioned from fluvial to lacustrine and deltaic (Stack et al., 2024).

The *Shuyak* and *Mageik* cores were collected from the *Amalik* outcrop (Figure 2; Table 2) in the *Amalik* member of the *Shenandoah* formation (Stack et al., 2024). The flat, dark coarse mudstones (Figure 2; Table 3) in *Amalik* were likely deposited aqueously at a stratigraphically low position at the front of the existing fan, likely in a fluvial setting (Stack et al., 2024) and then altered in the presence of water (Dehouck et al., 2023).

Table 3
Measurements of Grain Sizes and Shapes in Abraded Patches in WATSON Images of Abraded Patches

	Novarupta	Berry Hollow	Uganik Island	Thornton Gap
Mode ϕ*	4.4	4.5	3.9	2 and 4
Mean grain size ϕ	4.3	4.3	3.8	2.1
Sorting, standard deviation of ϕ	Well sorted, 0.35	Well sorted, 0.4	Moderately well-sorted, 0.74	Poorly sorted, 1.6
Grain shape	Equant	Subrounded	Equant	Subrounded to subangular

Note. $\phi = -\log_2(D)$, Where D is the diameter of a grain in millimeters.

The *Hazeltop* and *Bearwallow* cores were collected at *Wildcat Ridge* in the *Hogwallow Flats* member that consists of light-toned, fractured sedimentary rocks that are finer-grained than other rocks at the fan front (Tables 2 and 3; Figure 3). The *Hazeltop* core on this outcrop was drilled through a surface with multiple lumpy features and fractures, including a possible nodule (Figure 3). *Hidden Harbor*, an outcrop of the *Yori Pass* member of the *Cape Nukshak* region of the western Jezero fan front, is similarly light-toned, moderately sorted sandstone (Tables 2 and 3; Figure 4) and a likely lateral equivalent of the light-toned rocks at *Hogwallow Flats* and the similarly light-toned strata to the west of *Yori Pass* (Broz et al., 2023; Stack et al., 2024). The *Kukaklek* core from *Hidden Harbor* contains multiple veins and irregularly shaped bright features filled with anhydrite

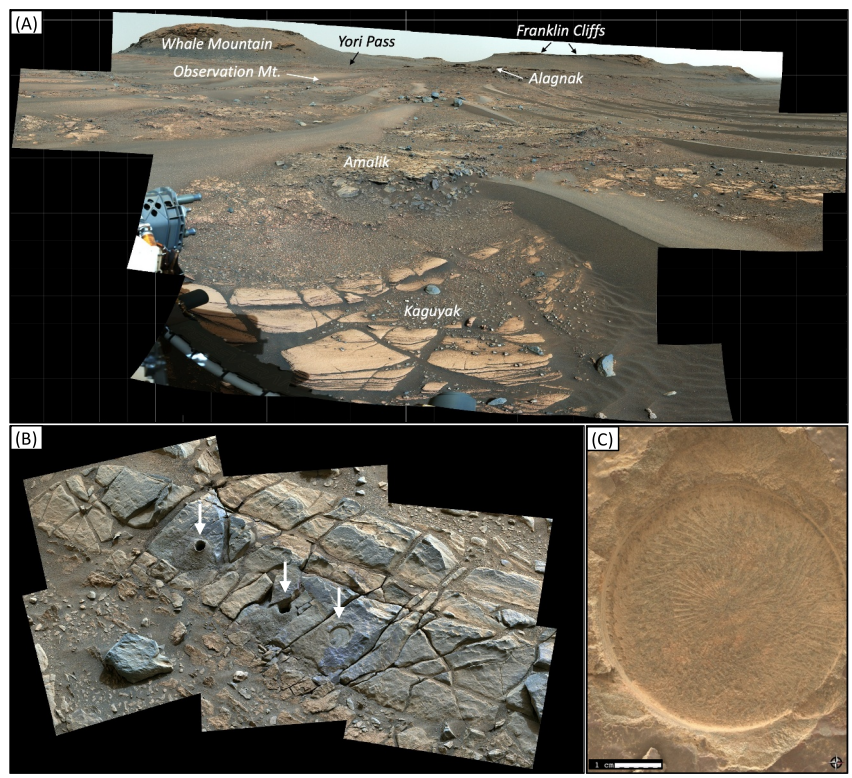

Figure 2. Local context of the *Amalik* outcrop and the *Novarupta* abrasion. (a) View of *Enchanted Lake* at the base of the *Alagnak* ridge within the lower *Cape Nukshak* fan front stratigraphy. The *Amalik* outcrop is located near the top of the exposed *Amalik* member, which underlies *Knife Creek and Alagnak*, and overlies the *Kaguyak* member. The *Amalik* outcrop is ∼5 m across; the vertical distance from *Amalik* to the upper surface of *Cape Nukshak* (the top of the *Alagnak* cliff) seen in this image is ∼4 m. *Franklin Hills* and *Whale Mountain* are parts of the fan. View is to the N; sol 425, zcam08450, Z110 enhanced color. *Observation Mountain* is the location of the regolith samples (*Atmo Mountain* and *Crosswind Lake*). A 3D model of the *Amalik* and *Enchanted Lake* area can be viewed at Tate (2023a). (b) The workspace after abrasion and sampling activities, showing the fracturing that occurred after *Shuyak* was cored (center arrow). The 5 cm wide *Novarupta abrasion* (right arrow), *Mageik* hole (left arrow). Sol 582, zcam08595, Z63 enhanced color. A 3D model of the Amalik workspace can be viewed at Tate (2023b). (c) Sol 568 WATSON 10-cm standoff focus merge of *Novarupta* abrasion. The diameter of the abrasion is 5 cm. A 3D model of the Novarupta abrasion patch can be viewed at Tate (2023c).

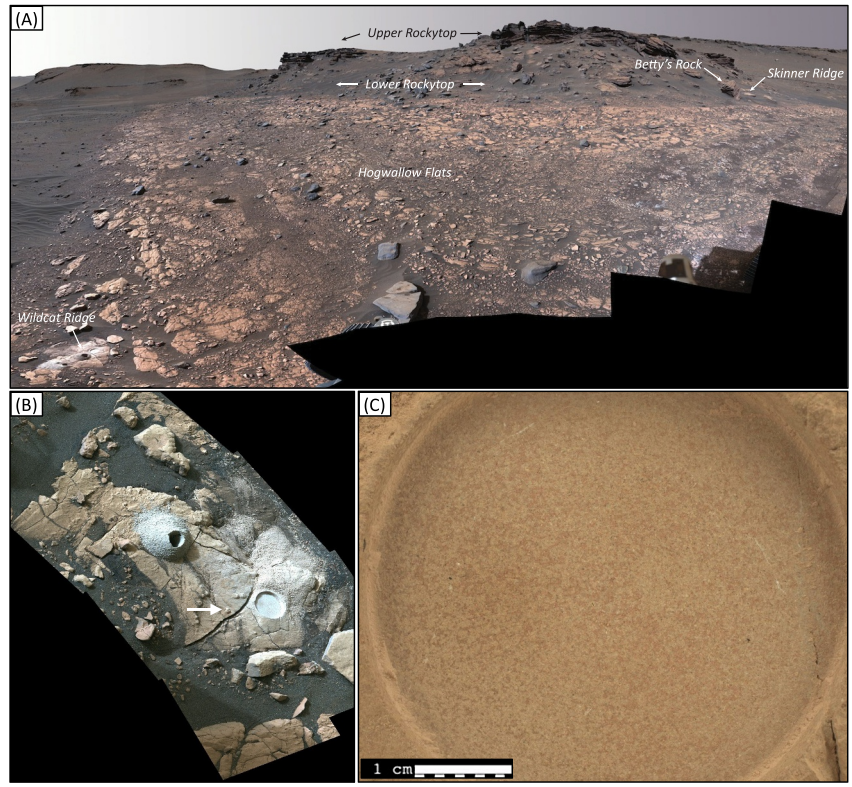

Figure 3. Local context of the *Wildcat Ridge* outcrop and the *Berry Hollow* abrasion. (a) The *Wildcat Ridge* outcrop viewed from the sampling workspace; View is to the NW; sol 518, zcam05842, Z034 enhanced color. *Wildcat Ridge* is located at the base of the exposed *Hogwallow Flats* member below *Lower Rockytop*. Lower stratigraphic units and crater floor lie below the bottom of the image. The *Wildcat Ridge* block is ∼0.4 m across. The *Skinner Ridge* block is ∼1 m across; the vertical distance from *Skinner Ridge* to the highest point of *Upper Rockytop* seen in this image is ∼6.5 m. (b) Mastcam-Z workspace image of *Wildcat Ridge* after sampling *Hazeltop* and abrasion of *Berry Hollow*. The white arrow points to a feature interpreted to be a concretion that is 1 cm long and 0.7 wide. The abrasion patch diameter is 5 cm. Sol 513, zcam08537, Z110 enhanced color. A 3D model of the Wildcat Ridge workspace can be viewed at Tate (2023d). (c) Sol 511 WATSON 7-cm standoff daytime image of *Berry Hollow* abrasion patch (5 cm wide). A 3D model of the Berry Hollow abrasion patch can be viewed at Tate (2023e).

(Figures 1 and 4). All these strata (Table 1) may have originated from the subaqueous downslope deposition of the materials into a stratified, hypersaline lake (Stack et al., 2024). Alternative interpretations invoke reworking, transport and subaerial deposition of these minerals (Benison et al., 2024).

The *Swift Run* and *Skyland* cores were collected from *Skinner Ridge*, an outcrop of the *Lower Rockytop* member of the *Hawksbill Gap* region of the western Jezero fan front (Figure 1; Stack et al., 2024). *Skinner Ridge* is a horizontally layered, medium-grained sandstone at the base of a scarp (Figure 5; Table 2). The observed sedimentary features (Stack et al., 2024), grain size distribution (Table 3) and the presence of a composite clasts and a cementing matrix around the grains support the interpretation of the *Swift Run* and *Skyland* cores as samples of a sandstone that was aqueously deposited at the front of the existing sediment fan and then altered and cemented in the presence of water.

3.2. Imaging and Compositional Analyses of Sampled Outcrops

All rocks sampled at Jezero fan front are hydrated and contain varying amounts of detrital minerals and minerals produced by aqueous alteration or precipitation from solution (Table 4; Dehouck et al., 2023; Figure S1 in Supporting Information S1). *Hogwallow Flats* and *Yori Pass* contain up to ∼20 wt% of SO_3 in hydrated Fe(II)/Mg sulfate minerals and some anhydrite, whereas *Skinner Ridge* and *Amalik* contain Fe/Mg carbonate minerals (Table 4; Figures S2–S5 in Supporting Information S1). The Mg/Fe(II) sulfate minerals in the matrix of

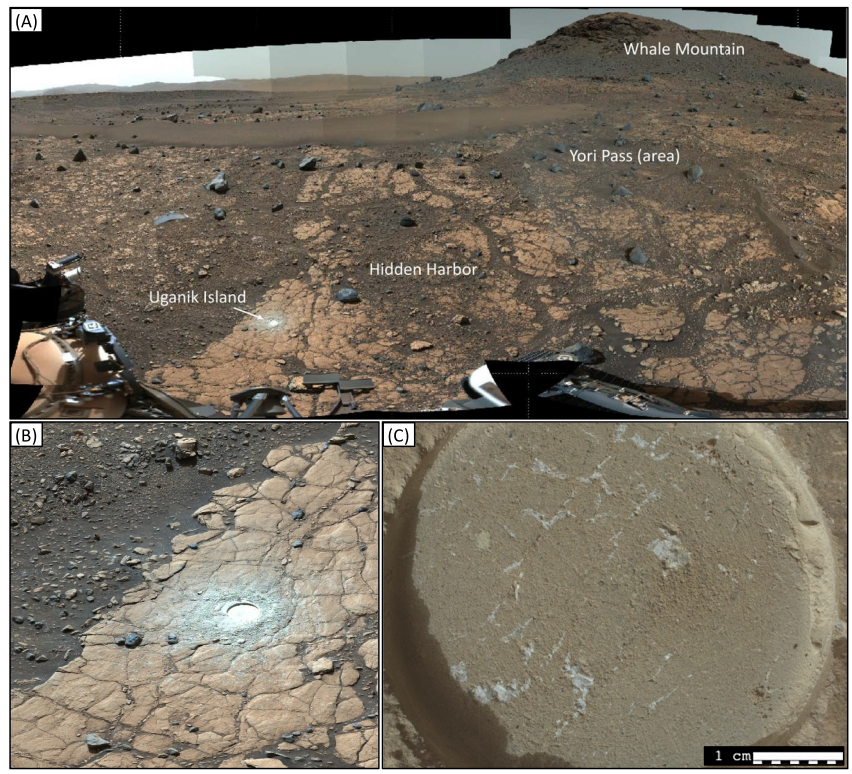

Figure 4. Local context of the *Hidden Harbor* outcrop and the *Uganik Island* abrasion. (a) The *Hidden Harbor* outcrop is located near the base of the exposed *Yori Pass* member. *Whale Mountain* (upper right) consists of stratigraphically higher fan units. Lower stratigraphic units and crater floor lie below the bottom of the image. The *Hidden Harbor* outcrop is ∼5 m across; the vertical distance from *Hidden Harbor* to the break in slope that defines the base of *Whale Mountain* seen in this image is ∼15 m. View is to the west; sol 619, zcam08623, Z110 enhanced color. The *Uganik Island* abrasion and *Kukaklek* coring location are indicated with white arrow. A 3D model of the Hidden Harbor area can be viewed at Tate (2023f). (b) The *Hidden Harbor* workspace on sol 619 after abrasion and prior to sampling; zcam08623 L0 enhanced color mosaic at a focal length of 34 mm. (c) Sol 612 WATSON 7-cm standoff focus merge of the *Uganik Island* abrasion (5 cm wide); most of the abrasion is in full sun illumination. A 3D model of the Uganik Island abrasion can be viewed at Tate (2023g).

Hogwallow Flats and *Yori Pass* are hydrated and lack Al, so they cannot be assigned to alunite-group sulfate minerals that contain ferric iron (Hurowitz et al., 2023; Figure S3 in Supporting Information S1). Anhydrous Ca sulfate minerals occur at *Amalik* (Table 4), whereas SuperCam and SHERLOC Raman spectroscopy detects anhydrite in the white veins and the lightest grains at *Yori Pass* and *Hogwallow Flats* (Table 4; Figure S2 in Supporting Information S1; Lopez-Reyes et al., 2023; Nachon et al., 2023). Based on the missing analytical totals in PIXL XRF analyses of the selected areas of the abraded surface, the abundances of elements that are not quantifiable by PIXL, such as H, C and N, and water are the highest in *Skinner Ridge* and the lowest in the sulfate-rich strata (Hurowitz et al., 2023; Supplementary Table 1). Some grains in *Skinner Ridge* and *Amalik* have compositions that are consistent with olivine and pyroxene (Figures S2 and S3 in Supporting Information S1). These two outcrops also contain various minor phases such as baddeleyite and ilmenite (Hurowitz et al., 2023; Table 4; Figure S3 in Supporting Information S1). *Skinner Ridge* exhibits the largest compositional heterogeneity and the most frequently detected Raman signatures of carbonate among the analyzed abraded patches (Table 4; Figures S4 and S5 in Supporting Information S1).

The absence of G-bands from the Raman spectra of all abraded patches indicates that organic concentrations are lower than the stated lower detection limit by Raman spectroscopy (0.1 wt%; Bhartia et al., 2021; Scheller et al., 2024). The UV luminescence by the SHERLOC instrument is more sensitive to aromatic organics (∼10 ppm detection limit, Bhartia et al., 2021; Razzell Hollis et al., 2022; Razzell Hollis et al., 2021). SHERLOC detected the doublet UV fluorescence centered at 305 and 325 nm in all sulfate-rich rocks that was the strongest in anhydrite veins and grains, and the luminescence centered at 330–350 nm in *Amalik* and *Skinner Ridge* (Table 4;

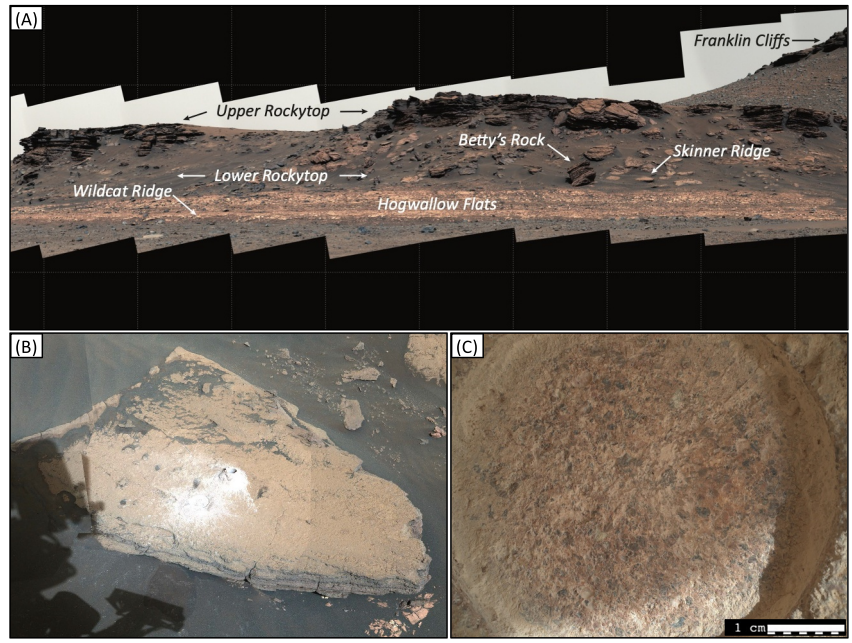

Figure 5. *Skinner Ridge* context and *Thornton Gap* abrasion. (a) View of the layered *Rockytop* ridge within the Hawksbill Gap fan front stratigraphy. The *Skinner Ridge* outcrop is located at the base of the *Lower Rockytop* unit above *Hogwallow Flats*. The *Franklin Cliffs* area in the upper right contains stratigraphically higher fan units. Lower stratigraphic units and crater floor lie below the bottom of the image. The *Skinner Ridge* block is ~1 m across; the vertical distance from *Skinner Ridge* to the highest point of *Upper Rockytop* seen in this image is ~6.5 m. View is to the NW; sol 459, zcam08479, Z110 enhanced color. (b) Workspace image after abrading *Thornton Gap* and sampling *Swift Run*. The abrasion patch is 5 cm across. Sol 492, zcam08517, Z034 enhanced color. A 3D model of the Skinner Ridge area can be viewed at Tate (2023h). (c) Sol 482 WATSON 7-cm standoff daytime image of *Thornton Gap* abrasion patch. A 3D model of the Thornton Gap abrasion can be viewed at Tate (2023i).

Supplemental Figures S4 and S5 in Supporting Information S1). Although this luminescence may be consistent with that of some 1- or 2-ring aromatic organics (Scheller et al., 2022; Sharma et al., 2023), it is even more consistent with the inorganic fluorescence of cerium in phosphate or sulfate (Gaft et al., 2015; Scheller et al., 2024; Shkolyar et al., 2021).

Table 4
Summary of Rock Geochemistry Measurements by the Combined Instrument Payload

	Novarupta	Berry Hollow	Uganik Island	Thornton gap
Minerals detected by PIXL XRF, SHERLOC Raman spectroscopy and SuperCam VISIR, LIBS and Raman[a,b,c]	Olivine, pyroxene, feldspar, serpentine, clay minerals, carbonates, sulfates, apatite, chromite, ilmenite, zircon/ baddeleyite	Hydrated and anhydrous sulfate minerals (anhydrite), phyllosilicates such as nontronite or saponite, ferric sulfates[2], some Ti- or Cr-oxides	Hydrated and anhydrous sulfate minerals (anhydrite), phyllosilicates such as nontronite or saponite, ferric sulfates, some Ti- or Cr-oxides, kaolinite or montmorillonite grains	Olivine, pyroxene, Fe/Mg carbonates, Fe/Mg clay minerals, hydrated silica or Al-OH minerals, minor Ca-phosphate, Ca-sulfate, Fe-Ti oxides and Fe-Cr oxide
Hydration by SuperCam VISIR and SHERLOC	Detected	Detected	Detected	Detected
Analytical totals by PIXL (wt%)	93.0	94.5	95.8	83.5
UV luminescence by SHERLOC	Centered at 330–340 nm	Doublet feature centered at 305–325 nm	Doublet feature centered at 305–325 nm	Centered at 285 nm and at 330–340 nm
Coatings[#]	Common	Absent	Absent	Reddish surface

[a]See Dehouck et al. (2023) for a synthesis of SuperCam data. [b]See Broz et al. (2023) for iron oxide detections by Mastcam-Z multispectral imaging. [c]See Hurowitz et al. (2023) for a synthesis of PIXL data.

4. Discussion

The rocks and materials sampled at Jezero fan front meet many science objectives of the Mars Sample Return Campaign (e.g., Beaty et al., 2019), including constraining the timing of and the reasons for Mars's climate change, volatile evolution and changing habitability and the search for potential signals of prebiotic or biological processes.

4.1. Preservation of Inorganic and Organic Biosignatures

Targeted search for organic compounds and potential biosignatures in the future returned samples may reveal a currently missing record of prebiotic chemistry and early life. To preserve abiotic, prebiotic or biological organic compounds and microbial fossils and textures from erasure, fast-precipitating minerals or clay- and silt-sized particles have to bind or encapsulate the organic features and protect them from being destroyed by oxidation, lysis, enzymatic degradation and radiolysis (e.g., Bosak et al., 2021; McMahon et al., 2018). Deposits that contain abundant clay minerals and precipitated fine-grained phases are particularly attractive targets in the search for organics and (pre)biosignatures because they enable the preservation of the morphological and chemical information by reducing chemical exchange and microbially-driven decay (e.g., Alleon et al., 2016; Moore et al., 2023). Clay minerals can also incorporate water and organic compounds (Lagaly et al., 2006). Hence, the search for indigenous organic compounds in the returned samples of aqueously deposited sedimentary rocks from Jezero would begin by analyses of the finest-grained clay-rich samples such as *Bearwallow* or *Hazeltop*. Rocks with the highest organic-preserving potential should also lack indicators of substantial post-depositional fluid flow and mineral dissolution and reprecipitation: oxidizing fluids that flow through the rocks modify or remove organic matter (Petsch et al., 2000; Sumner, 2004) by generating harder-to-analyze polymers and producing small organic acids and CO_2 (e.g., Benner et al., 2000; Chapiro, 1988; Fox et al., 2019). This criterion further increases the organic-preserving potential of *Bearwallow* and *Hazeltop* cores, which lack of large anhydrite grains and veins, over that of *Kukaklek*.

Samples from *Wildcat Ridge* have an additional advantage in that they lack indicators of either high-energy flow or exposure and desiccation, that is, environmental conditions that would prevent the settling of organic matter and impede microbial growth (Mariotti et al., 2014). However, Fe/Mg sulfate minerals detected in this outcrop (Table 4) indicate conditions that would challenge microbial growth because these minerals precipitate from very concentrated brines (Tosca et al., 2008; Wang et al., 2009). On Earth, they are reported mainly in salt efflorescences (e.g., Whittig et al., 1982) that do not support the growth of extensive modern microbial communities (Cockell, 2020; Macey et al., 2023). However, microbial extracellular polymers from hypersaline lakes and playas, when freeze-dried, can mediate the formation of sulfate and clay minerals including magnesium sulfate hexahydrate, talc and palygorskite and become encapsulated within such minerals (del Buey et al., 2021). The abundance of sulfate in *Wildcat Ridge* and its potential origin close to the photic zone may also enable the search for organic remnants of prebiotic processes. The synthesis of multiple classes of prebiotic molecules requires UV radiation (e.g., Karamian & Sharifnia, 2016; Patel et al., 2015; Powner et al., 2009; Xu et al., 2021), sulfite oxidized to sulfate (e.g., Green et al., 2021) and concentration that can occur by processes that can also promote the precipitation of Mg/Fe(II) sulfate minerals such as freezing or evaporation (e.g., Menor-Salván & Marín-Yaseli, 2012; Ross & Deamer, 2016). Although SHERLOC did not confidently detect organic compounds in any sulfate-rich or other sedimentary rocks (see below), some fluid or organic inclusions in sulfate crystals would be too small to be detected by the rover instruments (Benison et al., 2024; François et al., 2016). If present, such inclusions would present additional targets for astrobiological investigations of returned samples (Benison, 2019).

The 3.2 Ga old fluvial and tidally-influenced marine felsic sandstones and siltstones of the Moodies Group (Homann, 2019) provide a potential hydrodynamic analog of *Amalik*. Most sand beds in the Moodies Group do not preserve biosignatures, but some <1-mm-thick silica-rich surfaces from more quiescent, exposed intervals attest to the occasional growth and preservation of microbial mats under silica-rich conditions (Homann, 2019). If similarly thin silica-rich layers and textural biosignatures are present in *Amalik*, which was interpreted as a fluvial deposit (Stack et al., 2024), they would likely be obscured by surface coatings (Figure 2; Table 4) and not detectable during the analyses of bedding-parallel patches by the rover instrumentation.

4.2. Organic Detection

Given that one of the major objectives of the Mars 2020 mission is to find and collect materials that, among other potential biosignatures, preserve organic compounds (Farley et al., 2020), the astrobiological potential of the collected samples increases with their organic content. However, the SHERLOC instrument on Perseverance has not detected unambiguous organic signals to date (Scheller et al., 2024).

The SHERLOC instrument detects organic compounds in abraded patches by UV fluorescence and Raman spectroscopy (Bhartia et al., 2021; Scheller et al., 2022, 2024; Sharma et al., 2023). So far, SHERLOC has detected UV fluorescence consistent with ∼10 ppm small aromatics without an accompanying Raman feature centered at 1,600 cm^{-1} (Scheller et al., 2022; Sharma et al., 2023). The association of the detected UV fluorescence signals with specific mineral phases such as phosphates or sulfates (Scheller et al., 2022; Sharma et al., 2023) and dearth of potential organic Raman features motivates the need to better understand how SHERLOC detects organics (Scheller et al., 2024). Although this instrument can detect the UV fluorescence by some 1- or 2-ring aromatic compounds at $\sim 10^{-5}$ ppm or higher concentrations (Bhartia et al., 2021; Razzell Hollis et al., 2021), sulfate- and phosphate-associated cerium and silica defects are the current null hypotheses for the measured UV fluorescence signals (Gaft et al., 2015; Scheller et al., 2024). The report of only one potential, low-intensity Raman G-band by SHERLOC in thousands of points analyzed to date (Sharma et al., 2023) also suggests that organic concentrations in the acquired samples are lower than 0.1 wt% (Bhartia et al., 2021). All these uncertainties underscore the need for sample return and highly sensitive mass spectroscopy and nanoscale elemental mapping analyses similar to those used to confirm the presence of organic compounds and understand their abundances, spatial distribution and compositions in terrestrial samples (e.g., Alleon et al., 2021; Hickman-Lewis et al., 2016, 2018; Homann, 2019).

SHERLOC is much less sensitive to organics than the Sample Analysis at Mars instrument (SAM) on the Curiosity rover that relies on gas chromatography-mass spectrometry and evolved gas analysis to detect organic compounds at ppb concentrations. SAM found indigenous organic compounds in the lacustrine mudstones, sandstones and even dunes in Gale crater (Eigenbrode et al., 2018; Millan, Teinturier, et al., 2022; Millan, Williams, et al., 2022; Stern et al., 2022; Sutter et al., 2017; Szopa et al., 2020). The detection of high-molecular-weight organic compounds in various samples in Gale crater and the correlation of isotopically light methane with isotopically light sulfur in Cumberland mudstones (House et al., 2022) hint at diverse organic preservation pathways in martian rocks and soils and the complex cycling of organics between the martian atmosphere and soils (Franz et al., 2020). Laboratory analyses of the future returned rock and regolith samples using an array of spatially and compositionally resolved analytical methods could investigate these hints and mitigate various analytical issues related to the presence of oxychlorine species and leaked derivatization agents that challenged the organic detections by Curiosity (Eigenbrode et al., 2018; François et al., 2016; Mojarro et al., 2023).

The search for organic compounds in the future returned samples of aqueously deposited sedimentary rocks from Mars can also alleviate the depositional and contamination issues associated with martian meteorites. The two martian meteorites with ages >3 Ga, Northwest Africa (NWA) 7034 and Allan Hills (ALH) 84001 contain graphitized carbon (Steele et al., 2016), but these rocks have complex histories and were not deposited in a demonstrably habitable environment. ALH 84001 is igneous, heavily shocked and metamorphosed, and lacks a well constrained location of origin or geologic context. NWA 7034 and paired meteorites are polymict regolith breccias whose history involves the assembly of ∼4.4 Ga igneous clasts and annealing during moderate metamorphism within 1.5 Ga (Cassata et al., 2018). ALH 84001 has also been exposed to terrestrial fluids, organic compounds and microbes, that is, factors that complicate the quantification and characterization of extraterrestrial organic compounds (Bada et al., 1998; Glavin et al., 1999).

4.3. Effects of Ionizing Radiation

The time-integrated dose of ionizing radiation that a given sample has experienced through geologic time since deposition influences the preservation of organic matter. Ionizing radiation can destroy organic molecules, but can also polymerize and harden them by cross-linking (e.g., Chapiro, 1988; Fox et al., 2019; Trojanowicz, 2020). Ionizing radiation has three known sources: (a) solar ultraviolet (UV) radiation, (b) galactic cosmic ray (GCR) particles and (c) radioactive decays of K, U, and Th in the host rock. Each of these radiation sources has a different rate of production, depth attenuation beneath the rock surface on Mars, and dependence on sample composition. UV solar radiation effects attenuate in solid rocky materials over very short distances (∼mm) beneath the rock

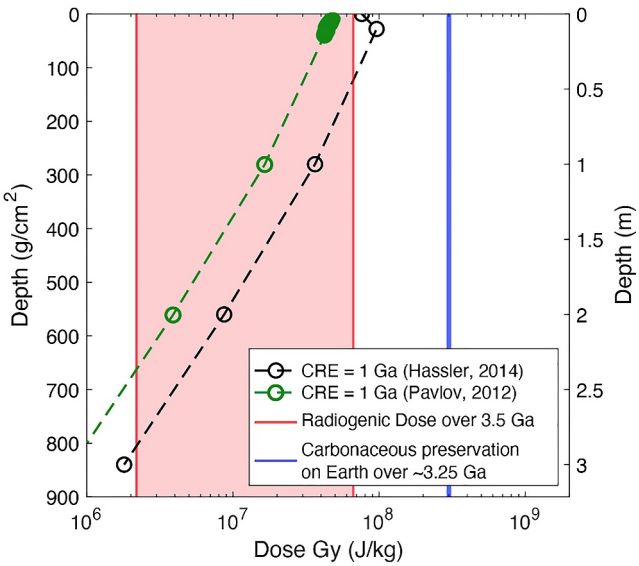

Figure 6. In situ cosmic ray and radiogenic ionizing radiation dose estimates for samples collected from the sedimentary fan front. Depth-dependent radiation doses are shown using dose rate estimates of Hassler et al. (2014) in black and Pavlov et al. (2012) in green, assuming a cosmic ray exposure (CRE) duration of 1 Ga and a constant galactic cosmic ray flux to the surface of Mars for all time since exposure. Time-integrated radiogenic dose from U, Th and K decays over the last 3.5 Ga are shown (red) for K_2O ranging from 0.1 to 3.0 weight percent and assumed K/U and K/Th ratios. For comparison, we estimate the time-integrated radiogenic dose experienced by rocks of the Barberton Greenstone Belt (blue) that preserve carbonaceous lamination (e.g., Hickman-Lewis et al., 2018).

surface (Cockell & Raven, 2004), such that both the abrasion and core depths avoid material that has been modified by this known radiation source since sediment deposition. GCR particles and their associated radiation damage effects in solids are deeper and known to attenuate solid rocky materials with a characteristic (i.e., *e*-folding) length scale of ~160 g/cm^2 (~0.5 m; Gosse & Phillips, 2001). The flux of GCR particles to the surface of Mars has likely varied through time, as influenced by changes in solar activity, the atmospheric thickness and any magnetic field on Mars over long timescales (Gosse & Phillips, 2001). However, given the attenuation length scale in rocky material, the mean, time-integrated dose of GCR irradiation since a given sample was either progressively exhumed (i.e., via surface erosion processes) or instantaneously exposed (e.g., after a landslide or impact) to within the uppermost few meters of the rock surface would provide the primary control on organic molecule preservation. Observations of Mars' surface radiation by the Radiation Assessment Detector on Curiosity (Hassler et al., 2014) provide an estimate of the modern GCR dose rate expected for the samples collected from the Jezero Fan.

Using the simplifying assumptions that: (a) the dose rate observed at surface at Gale Crater (~0.01 Gy/yr) also applies to Jezero crater, (b) the GCR energy distribution attenuates with depth as estimated by Pavlov et al. (2012) and Hassler et al. (2014), and (c) that the modern GCR flux was constant through all time, we estimate the total ionizing energy dose in Gy (J/kg) as a function of shielding beneath the rock surface, and for an assumed exposure duration of 1 Ga (Figure 6). Although the exposure duration is presently unknown, we consider 1 Ga to be a conservative estimate; the apparent scarp at the fan front and the erosional processes active today both indicate that the exposed rocks were likely exhumed long after their initial deposition time. Each sample's exposure duration can ultimately be constrained by observations of stable cosmogenic nuclides in Earth laboratories; greater or lesser durations predict correspondingly higher or lower ionizing energy doses, respectively, but with similar attenuations with depth. Owing to depth dependence of the GCR dose, recently exposed samples, such as the samples collected from the degrading/buried fan units, will have accumulated a GCR dose only prior to deposition (e.g., during sediment transport) and after exhumation. If organic compounds were incorporated into the rocks at the time of sediment deposition, only the latter dose is relevant and indicates that the samples from Jezero fan front can preserve organic compounds. Given that the erosional remnants (e.g., Goudge et al., 2015; Mangold et al., 2021; Schon et al., 2012) indicate that the western fan was formerly larger, and that its now eroded strata would have shielded the currently exposed and sampled rocks at the fan front, the samples are unlikely to have experienced maximum time-integrated GCR doses shown in Figure 6.

Unlike solar UV and GCR doses, the time-integrated ionizing radiation due to radioactive decay of K, U, and Th in the host rock should not depend on depth, provided the concentrations of these radioactive elements do not vary with depth. To estimate the cumulative radiogenic dose due to radioactive decays along the ^{238}U, ^{235}U and ^{232}Th decay series, and ^{40}K within the rocks, we use the approximate range of K_2O observed in the four abrasions (0.1–3.0 wt%), assume K/U and K/Th molar ratios of 1.2×10^5 and 3.2×10^4, respectively (Martin et al., 2020), and calculate the total dose over 3.5 Ga (that is, since an assumed timing of sediment deposition; (Mangold et al., 2020)). Greater or lesser durations since deposition predict correspondingly higher or lower doses, respectively (Figure 6).

These estimates indicate that the doses expected for GCR exposure and inherent to the rocks collected from the Jezero fan are largely unavoidable and subequal for the anticipated exposure durations for each (Figure 6). Importantly, the combined estimates for both sources amount to a smaller dose than that estimated for sedimentary rocks of the Fig Tree Group from the ~3.25 Ga Barberton greenstone belt, assuming 6 wt% K_2O, 8 ppm U and 27 ppm K (Hofmann, 2005). In spite of the higher GCR doses and greenschist metamorphism, terrestrial rocks of this age preserved carbonaceous materials of demonstrably biogenic origin (Hickman-Lewis et al., 2016, 2018; Homann, 2019; van Zuilen et al., 2007), supporting the potential of samples acquired by the Perseverance

rover to preserve organic material. Thus, although the centimeters-long cores sample only up to 8 cm below the currently exposed rocks at the Jezero fan front, these samples should be able to preserve organic compounds. The recognized sensitivity of organic compounds to ionizing radiation and heat requires that the returned samples used to search for and analyze organic compounds not be sterilized by either method upon return to Earth (Velbel et al., 2021), if the sample safety assessment of the returned samples determines that the samples can be released without sterilization.

4.4. Records of Changing Planetary Habitability

Since Mariner 9 returned the first images of Martian water-carved channels in the early 1970s, subsequent sample, orbital and rover studies have provided evidence for water as an important geological and geochemical agent on Mars's surface. This evidence has inspired questions of when and how Mars dried, how much water it contained, how warm its surface was, and when and why its climate changed (Bibring et al., 2005, 2006; Carr & Head, 2010; Fassett and Head, 2008; McLennan et al., 2019; Poulet et al., 2005; Scheller et al., 2021; Squyres et al., 2004; Wordsworth, 2016). Isotopic analyses of water in Martian meteorites have provided some constraints on the cycling of crustal and magmatic water (e.g., Barnes et al., 2020; Greenwood et al., 2008; Leshin, 2000; Leshin et al., 1996; Usui et al., 2012, 2015). Analyses of minerals that precipitate in water or in its presence, such as carbonates, hydrated sulfates and clay minerals, as well as other volatiles such as chlorine, can now help answer these questions, revolutionize reconstructions of atmospheric and hydrological processes across past habitable environments on Mars (e.g., Achilles et al., 2020; Grotzinger et al., 2005, 2014; McLennan et al., 2005) and probe Mars's evolving habitability.

Limestone and dolostone deposits are common on Earth, where the active water and tectonic cycles reduce the abundances of the more soluble sulfate minerals. This pattern is reversed on Mars (King & McLennan, 2010; Murchie et al., 2009), where sulfate and clay minerals are hypothesized as major reservoirs of water equivalent hydrogen (Feldman, Mellon, et al., 2004; Feldman, Prettyman, et al., 2004; Maurice et al., 2011; Scheller et al., 2021; Vaniman et al., 2004; Wang et al., 2016) that also record past and present environmental conditions such as the water availability, pH and salinity (e.g., Bristow et al., 2015; Karunatillake et al., 2014; Vaniman et al., 2018). Assuming that water accounts for the entire 5 wt% of the missing analytical total measured in whole scans by PIXL in the sulfate-rich samples from *Wildcat Ridge*, the respective volumes of the *Hazeltop* and *Bearwallow* cores from this outcrop (Tables 1 and 4), may store from 0.8 to 1.2 g or about a milliliter of water, assuming 2–2.8 g/cm^3 as the average density (Deer et al., 1966). Phyllosilicates that coexist with hydrated Mg/Fe sulfates at *Wildcat Ridge* and *Yori Pass* (Table 4) may also act as a water buffer and prevent the dehydration of the latter minerals (Wilson & Bish, 2012). The total volume of *Kukaklek* and the analytical totals measured on *Uganik Island* allow for up to 0.8 g of water (Tables 1 and 4). Notably, terrestrial laboratories can analyze nanoliter-volume water samples (e.g., Morrison et al., 2001). Both the specific types and hydration states of the collected sulfate phases would likely be altered both on the rover and upon sample return owing to the temperature and humidity changes. Given that all rock cores from Jezero fan front are hydrated and may contain other volatiles (e.g., Williams et al., 2016), redox-sensitive elements such as iron and cerium and biogenic elements, sterilization of the future returned subsamples by heat or ionizing radiation would likely modify the original signals of various processes (Velbel et al., 2021).

Isotopic analyses of sulfur in sulfate minerals can also be used to reconstruct atmospheric photochemistry and the interactions of the martian crust and the mantle (Thiemens et al., 2001), particularly when coupled with the analyses of coeval igneous and sedimentary sulfide minerals (e.g., Ono, 2017). Sulfide mineral grains in sedimentary rocks can be much smaller than the detection limit of instruments on the Perseverance (e.g., Gregory et al., 2015; Ono et al., 2009), so their detection and analyses await sample return. If micrometer-scale pyrite and similar grains are present in these rock cores, sulfur isotopes in such grains can preserve additional isotopic imprints of local biological processes such as microbial sulfate reduction (Sim et al., 2011; Ueno et al., 2008).

Carbonate minerals in martian meteorites provide information about the pH, fluid chemistry, fluid temperatures, water activity, and the timing of fluid flow and carbonate precipitation (Borg et al., 1999; Bridges et al., 2001; Eiler et al., 2002; Halevy et al., 2011; Niles et al., 2005; Valley et al., 1997). Carbonates account for only about 1 volume % in ALH 84001 (Bridges et al., 2001; Mittlefehldt, 1994) and for 16 to 34 wt% of some olivine- and pyroxene-rich outcrops in Gusev crater (Morris et al., 2010). The low analytical totals of *Novarupta* and *Thornton*

Gap, 93 wt% and 83.5 wt%, respectively, and the detections of carbonate minerals in these abrasions (Table 4) indicate that the corresponding samples (Table 1) contain more carbonate than ALH 84001. Assuming a density lower than that of Martian basaltic rocks and comparable to that of terrestrial basalts, 2.9 g/cm^3, the missing analytical totals from *Novarupta* (Table 4) in *Mageik* (10.4 cm^3) and *Shuyak* (7.8 cm^3) are consistent with up to 2.1 and 1.5 g of carbonate, respectively. Applying the same assumptions to *Thornton Gap*, we estimate up to 4.5 and 4 g of carbonate, in *Swift Run* and *Skyland* (Table 4). These are the upper limits because hydration and any potential organic carbon and nitrogen-bearing phases may account for some of the missing analytical totals.

Resolving the duration of hydrological activity in Jezero crater is imperative to understanding its past habitability and astrobiological potential. In the absence of extensive, permanent and interconnected bodies of water, transiently habitable, yet uninhabited environments may exist due to the infrequent or sparse influx of microbial inocula or feedstock molecules for prebiotic reactions (Cockell, 2020, 2021). If Jezero harbored only short-lived habitable environments, then only low levels of organics and few, if any, potential biosignatures are expected. If, instead, early habitable environments were widespread and connected in space and time, analyses of all returned rocks that were deposited under similar geochemical and flow conditions may reveal similar organic, morphological and isotopic features.

Analyses of the inorganic components of samples acquired in Jezero crater and its fan front are key to addressing the timing and duration of habitable conditions and testing any causal relationships among the evolution of magnetic field, past climate conditions, aqueous activity and surface chemistry. Crystallization ages of mechanically-separable detrital igneous clasts (i.e., >250 μm) from *Skinner Ridge* can provide upper bounds on the timing of fan sediment deposition and therefore the permissible timing of Lake Jezero, as can the constraints from geochronology of underlying *Seitah* samples (Simon et al., 2023). Isotopic geochronology (e.g., K-Ar, U-Th-Pb, Rb-Sr) and thermochronology based on, for example, ^{40}Ar/^{39}Ar or (U-Th)/He, can reconstruct the ages and crustal exhumation histories prior to the transport and deposition of feldspar, pyroxene, and possibly phosphates, carbonates and Fe-oxides identified in *Skinner Ridge*.

Geochronology of post-depositional phases within these samples, including cements and chemical weathering products, using a variety of geochronology methods (e.g., K-Ar, U-Th-Pb, Rb-Sr, U-Th/He) can constrain the timing of alteration and cementation of the fan sediments and late-stage aqueous activity. Such information would place a *lower* bound on the timing of sediment and fan deposition. With the more recent collection of other cement-containing coarse-grained samples from higher in the fan stratigraphy (e.g., *Otis Peak* and *Pilot Mountain* samples), it may be possible to place closer constraints on the duration of fluvio-lacustrine habitable conditions in Jezero crater.

Samples from *Wildcat Ridge* are not well-suited for existing methods of isotopic geochronology. This is one of the reasons why a fine-grained sedimentary rock was collected in close association with a coarser sedimentary rock (e.g., *Skinner Ridge*): the latter can be used to constrain the deposition timing of *Wildcat Ridge*. However, it may be possible for existing methods of isotopic geochronology to be applied or refined to constrain the timing of sulfate precipitation. In addition to quantifying the timing of late-stage aqueous activity, such information would place a lower bound on the timing of sediment and fan deposition. Observations of stable cosmogenic nuclides (e.g., ^{3}He, ^{21}Ne, ^{36}Ar, ^{38}Ar) in bulk *Hazeltop* and *Bearwallow* samples (Table 1) could also quantify the material's integrated cosmic ray exposure duration, thereby helping to constrain the latest-stage erosional history of the fan.

The presence of Ti-Fe and Ti-Cr-Fe grains in *Skinner Ridge* and *Amalik* (Table 4) suggests that the cores contain ferromagnetic minerals at and below the spatial scales detectable by rover instruments. These minerals may enable relative temporally resolved measurements of the relative paleointensity of the martian dynamo (Mittelholz et al., 2018) and complement measurements of magnetism in igneous rocks from the floor of Jezero crater (Simon et al., 2023). In combination with geochronology, this could constrain the timing of the martian paleomagnetic field to test the hypothesis that the cessation of an early dynamo led to loss of an early Martian atmosphere and the subsequent drying and cooling of Mars (Egan et al., 2019; Ehlmann et al., 2016). The orientations of the samples (Weiss et al., 2024) should enable the first measurements of the paleodirection of the magnetic field, the first for any planetary body besides Earth and a conglomerate test (Graham, 1949) to determine if the samples retained magnetization prior to, or after, deposition and constrain their thermal and diagenetic histories.

5. Conclusions

The Perseverance rover collected seven absolutely oriented samples of rocks at the Jezero fan front: two aqueously deposited sandstones from the Jezero fan front, a sulfate- and clay-rich mudstone from a distinct, laterally extensive deposit along the fan front, samples of regolith and a single sample of a sulfate-rich sandstone. Two witness tubes were sealed as controls for earth-sourced contamination by the rover. A suite of nine sedimentary, igneous, regolith and atmospheric samples collected during the Crater Floor and Fan Front Campaigns and one witness tube were deposited at the *Three Forks Cache* in January 2023 (https://mars.nasa.gov/mars-rock-samples/#20). A matching sample suite that remains on the rover has grown with the addition of rocks from the fan top, carbonate-rich rocks from the marginal deposits in the crater and the planned addition of rocks from the areas outside of the crater.

Aqueously deposited and altered rocks, from known locations and with a well-constrained geological context, contain water, a variety of precipitated minerals such as sulfates and carbonates and detrital clay and igneous minerals. The *Hazeltop* and *Bearwallow* samples have the highest astrobiological potential due to their small grain sizes and the abundance of hydrated sulfate phases and clay minerals. These phases preserve volatiles such as water and can also preserve organic inclusions and organic compounds. The *Kukaklek* core has a lower astrobiological potential relative to the *Hazeltop* and *Bearwallow* cores because it contains grains with larger average sizes and more pervasive evidence for later fluid flow. Organic compounds were not conclusively detected in these and other samples acquired during the Fan Front Campaign, which motivates analyses by the much more sensitive terrestrial instruments in future returned samples. Thus, future sample-receiving facilities should consider the impact of potential sterilization treatments on volatiles and organic compounds in any returned samples.

The coarser-grained mudstones and sandstones such as *Amalik* and *Skyland*/*Swift Run* would have the lowest likelihood of preserving local organic matter and potential textural biosignatures, but contain carbonate minerals and detrital grains that are key to constraining the weathering processes in the watershed and on the fan and the timing and duration of aqueous activity in the fan, Martian dynamo and regional hydrology and climate. Within these samples, the highest astrobiological potential belongs to the fine-grained Fe- and Mg-containing matrix that cemented composite grains in fluids upstream of *Skinner Ridge*.

Analyses of the returned materials in terrestrial laboratories would provide the currently unavailable organic, isotopic, chemical, morphological, geochronological and paleomagnetic records of the coupled evolution of Mars's water, carbon, redox and climate cycles. These analyses would engage an exceptionally broad scientific community and expand the value of returned samples beyond the realm of meteoritics, rover science and planetary science.

Conflict of Interest

The authors declare no conflicts of interest relevant to this study.

Data Availability Statement

Data acquired by various instruments on the Perseverance rover were used to describe the samples. All data are publicly available at PDS (https://pds.nasa.gov) 6 months after the acquisition. Software developed for each instrument implements appropriate calibrations and is used to process and visualize the data. OpenSource version of Pixlise/Piquant software used by PIXL is available on Zenodo at https://zenodo.org/records/6959126#.YvrZpnbMJPY and is referenced under Barber (2022) in the References section. The Initial Reports that describe the characteristics of the samples available at the time of sampling and described in the study are available through Open Access at https://pds-geosciences.wustl.edu/missions/mars2020/returned_sample_science.htm. via https://doi.org/10.17189/49zd-2k55. This publication describes samples 11–20 and is referenced as Shuster et al. (2023) in the Initial Report available at: https://pds-geosciences.wustl.edu/m2020/urn-nasa-pds-mars2020_sample_dossier/initial_reports/initial_reports_volume2.pdf. The 3D models of the abraded patches and outcrops analyzed at Jezero Fan Front are available at Sketchfab and referenced as Tate (2023a, 2023b, 2023c, 2023d, 2023e, 2023f, 2023g, 2023h, 2023i) [3D Visualization] in the References section.

Acknowledgments
We wish to thank all members of the Perseverance rover engineering and science teams. T. B., D.L.S., J.I.S., B.P.W., E.N.M., K.C.B., A.D.C., E.M.H., L.E.M., B.A.C., A.H.T., A.J.B., J.W.R.Jr. and A.U. were supported by the NASA Mars Exploration Program. T.B. was supported by the Miller Institute Fellowship and the Simons Foundation Collaboration on the Origins of Life. E.L.S. was supported by a postdoctoral fellowship from the Heising-Simons Foundation. S.S. was supported by the Swedish National Space Agency. K.M. S's, KAF's, J.N.M.'s, K.P.H.'s, A.C.A's, F. C. III's, J.I.N.'s, S.S.'s and K.U.'s effort was carried out at the Jet Propulsion Laboratory, California Institute of Technology under a contract with the National Aeronautics and Space Administration. C. D. K. H. and N.R. were supported by the Canadian Space Agency. K.H.-L. and M.A.S. were supported the UK Space Agency. M.-P.Z. was supported by MCIN/AEI (Spain), L. M., J.R.J., S.M., R.C.W., K.B., S.B., O.B., G.C., E.C., A.C., E.D., O.F., T.F., H.K., and C.R. were supported by the Mars Exploration Program and Le Centre National de la Recherche Scientifique (CNRS) and Centre National d'Etudes Spatiales (CNES) grants to SuperCam. K.H., K.H. W., M.E.M., B.V.W., D.K.B., A.S. and A. W. were supported by the Mars Exploration Program grants to SHERLOC/ WATSON. A.C.A., M.L.C., D.C.C., J.A. H., D.A.K.P. were supported by the Mars Exploration Program grants to PIXL. J.E. C. and E.G. were supported by The Natural Sciences and Engineering Research Council of Canada and the Canadian Space Agency, A.G.F. was supported by the European Research Council, Consolidator Grant 818602, D. T. Flannery was supported by an Australian Research Council Grant, T. F. was supported by ASI/INAF, F.G.G. was supported by INTA internal project DAXE. S.G. is supported by UK Space Agency and Royal Society. G.L.R. is supported by The Ministry of Economy and Competitiveness (MINECO, Spain).

References

Achilles, C., Rampe, E., Downs, R., Bristow, T. F., Ming, D. W., Morris, R. V., et al. (2020). Evidence for multiple diagenetic episodes in ancient fluvial-lacustrine sedimentary rocks in Gale crater, Mars. *Journal of Geophysical Research: Planets*, *125*(8), e2019JE006295. https://doi.org/10.1029/2019je006295

Alleon, J., Bernard, S., Le Guillou, C., Daval, D., Skouri-Panet, F., Pont, S., et al. (2016). Early entombment within silica minimizes the molecular degradation of microorganisms during advanced diagenesis. *Chemical Geology*, *437*, 98–108. https://doi.org/10.1016/j.chemgeo.2016.05.034

Alleon, J., Bernard, S., Olivier, N., Thomazo, C., & Marin-Carbonne, J. (2021). Inherited geochemical diversity of 3.4 Ga organic films from the Buck Reef Chert, South Africa. *Communications Earth & Environment*, *2*(1), 6. https://doi.org/10.1038/s43247-020-00066-7

Alleon, J., & Summons, R. E. (2019). Organic geochemical approaches to understanding early life. *Free Radical Biology and Medicine*, *140*, 103–112. https://doi.org/10.1016/j.freeradbiomed.2019.03.005

Allwood, A. C., Rosing, M. T., Flannery, D. T., Hurowitz, J. A., & Heirwegh, C. M. (2018). Reassessing evidence of life in 3,700-million-year-old rocks of Greenland. *Nature*, *563*(7730), 241–244. https://doi.org/10.1038/s41586-018-0610-4

Allwood, A. C., Wade, L. A., Foote, M. C., Elam, W. T., Hurowitz, J. A., Battel, S., et al. (2020). PIXL: Planetary instrument for X-ray lithochemistry. *Space Science Reviews*, *216*(8), 1–132. https://doi.org/10.1007/s11214-020-00767-7

Allwood, A. C., Walter, M. R., Kamber, B. S., Marshall, C. P., & Burch, I. W. (2006). Stromatolite reef from the early Archaean era of Australia. *Nature*, *441*(7094), 714–718. https://doi.org/10.1038/nature04764

Anderson, R. B., Forni, O., Cousin, A., Wiens, R. C., Clegg, S. M., Frydenvang, J., et al. (2022). Post-landing major element quantification using SuperCam laser induced breakdown spectroscopy. *Spectrochimica Acta Part B: Atomic Spectroscopy*, *188*, 106347. https://doi.org/10.1016/j.sab.2021.106347

Bada, J. L., Glavin, D. P., McDonald, G. D., & Becker, L. (1998). A search for endogenous amino acids in Martian meteorite ALH84001. *Science*, *279*(5349), 362–365. https://doi.org/10.1126/science.279.5349.362

Barber, T. (2022). pixlise/piquant: 2.0 open source migration release (v2.0) [Software]. *Zenodo*. https://doi.org/10.5281/zenodo.6959126

Barnes, J. J., McCubbin, F. M., Santos, A. R., Day, J. M., Boyce, J. W., Schwenzer, S. P., et al. (2020). Multiple early-formed water reservoirs in the interior of Mars. *Nature Geoscience*, *13*(4), 260–264. https://doi.org/10.1038/s41561-020-0552-y

Beaty, D. W., Grady, M. M., McSween, H. Y., Sefton-Nash, E., Carrier, B. L., Altieri, F., et al. (2019). The potential science and engineering value of samples delivered to Earth by Mars sample return: International MSR Objectives and Samples Team (iMOST). *Meteoritics & Planetary Sciences*, *54*(S1), S3–S152. https://doi.org/10.1111/maps.13242

Bell, J., Maki, J., Mehall, G., Ravine, M., Caplinger, M., Bailey, Z., et al. (2021). The Mars 2020 Perseverance rover mast camera zoom (Mastcam-Z) multispectral, stereoscopic imaging investigation. *Space Science Reviews*, *217*, 1–40. https://doi.org/10.1007/s11214-020-00755-x

Benison, K. C. (2019). How to search for life in martian chemical sediments and their fluid and solid inclusions using petrographic and spectroscopic methods. *Frontiers in Environmental Science*, *7*, 108. https://doi.org/10.3389/fenvs.2019.00108

Benison, K. C., Gill, K. K., Allwood, A. C., Bosak, T., Broz, A., Clark, B. C., et al. (2024). Depositional and diagenetic sulfates of Hogwallow Flats and Yori Pass, Jezero crater: Potential for preserved environmental indicators and possible biosignatures from past martian surface waters and groundwaters. *Journal of Geophysical Research: Planets*, *129*(2), e2023JE008155. https://doi.org/10.1029/2023je008155

Benner, S. A., Devine, K. G., Matveeva, L. N., & Powell, D. H. (2000). The missing organic molecules on Mars. *Proceedings of the National Academy of Sciences*, *97*(6), 2425–2430. https://doi.org/10.1073/pnas.040539497

Bernard, S., Criouet, I., & Alleon, J. (2021). Recognizing Archean traces of life: Difficulties and perspectives. In D. Alderton & S. A. Elias (Eds.), *Encyclopedia of geology* (2nd ed., pp. 211–219). Academic Press.

Bhartia, R., Beegle, L. W., DeFlores, L., Abbey, W., Razzell Hollis, J., Uckert, K., et al. (2021). Perseverance's scanning habitable environments with Raman and luminescence for organics and chemicals (SHERLOC) investigation. *Space Science Reviews*, *217*(4), 58. https://doi.org/10.1007/s11214-021-00812-z

Bibring, J.-P., Langevin, Y., Gendrin, A., Gondet, B., Poulet, F., Berthé, M., et al. (2005). Mars surface diversity as revealed by the OMEGA/Mars Express observations. *Science*, *307*(5715), 1576–1581. https://doi.org/10.1126/science.1108806

Bibring, J.-P., Langevin, Y., Mustard, J. F., Poulet, F., Arvidson, R., Gendrin, A., et al. (2006). Global mineralogical and aqueous Mars history derived from OMEGA/Mars Express data. *Science*, *312*(5772), 400–404. https://doi.org/10.1126/science.1122659

Borg, L. E., Connelly, J. N., Nyquist, L. E., Shih, C.-Y., Wiesmann, H., & Reese, Y. (1999). The age of the carbonates in Martian meteorite ALH84001. *Science*, *286*(5437), 90–94. https://doi.org/10.1126/science.286.5437.90

Bosak, T., Moore, K. R., Gong, J., & Grotzinger, J. P. (2021). Searching for biosignatures in sedimentary rocks from early Earth and Mars. *Nature Reviews Earth & Environment*, *2*(7), 490–506. https://doi.org/10.1038/s43017-021-00169-5

Bridges, J. C., Catling, D., Saxton, J., Swindle, T., Lyon, I., & Grady, M. (2001). Alteration assemblages in Martian meteorites: Implications for near-surface processes. *Space Science Reviews*, *96*, 365–392. https://doi.org/10.1007/978-94-017-1035-0_13

Bristow, T. F., Bish, D. L., Vaniman, D. T., Morris, R. V., Blake, D. F., Grotzinger, J. P., et al. (2015). The origin and implications of clay minerals from Yellowknife Bay, Gale crater, Mars. *American Mineralogist*, *100*(4), 824–836. https://doi.org/10.2138/am-2015-5077ccbyncnd

Broz, A. P., Horgan, B. H., Kalucha, H., Garczynski, B., Haber, J., Dehouck, E., & Mastcam-Z Team. (2023). Diagenetic alteration of Hogwallow flats, Jezero crater, Mars. *Paper presented at the 54th Lunar and Planetary Science Conference 2023: The Woodlands, Texas*.

Carr, M. H., & Head, J. W. III. (2010). Geologic history of Mars. *Earth and Planetary Science Letters*, *294*(3–4), 185–203. https://doi.org/10.1016/j.epsl.2009.06.042

Cassata, W. S., Cohen, B. E., Mark, D. F., Trappitsch, R., Crow, C. A., Wimpenny, J., et al. (2018). Chronology of martian breccia NWA 7034 and the formation of the martian crustal dichotomy. *Science Advances*, *4*(5), eaap8306. https://doi.org/10.1126/sciadv.aap8306

Chapiro, A. (1988). Chemical modifications in irradiated polymers. *Nuclear instruments and methods in physics research Section B: Beam interactions with materials and atoms*, *32*(1–4), 111–114. https://doi.org/10.1016/0168-583x(88)90191-7

Cockell, C. S. (2020). Persistence of habitable, but uninhabited, aqueous solutions and the application to extraterrestrial environments. *Astrobiology*, *20*(5), 617–627. https://doi.org/10.1089/ast.2019.2179

Cockell, C. S. (2021). Are microorganisms everywhere they can be? *Environmental Microbiology*, *23*(11), 6355–6363. https://doi.org/10.1111/1462-2920.15825

Cockell, C. S., & Raven, J. A. (2004). Zones of photosynthetic potential on Mars and the early Earth. *Icarus*, *169*(2), 300–310. https://doi.org/10.1016/j.icarus.2003.12.024

Deer, D. A., Howie, R. A., & Zussman, J. (1966). *An introduction to the rock forming minerals*. Longman Scientific & Technical.

Dehouck, E., Forni, O., Quantin-Nataf, C., Beck, P., Mangold, N., Royer, C., & the SuperCam team. (2023). Overview by the bedrock chemistry and mineralogy observed by the SuperCam during Perseverance's Delta Front Campaign. *Paper presented at the 54th Lunar and Planetary Science Conference, The Woodlands, TX*.

del Buey, P., Sanz-Montero, M. E., Braissant, O., Cabestrero, Ó., & Visscher, P. T. (2021). The role of microbial extracellular polymeric substances on formation of sulfate minerals and fibrous Mg-clays. *Chemical Geology*, *581*, 120403. https://doi.org/10.1016/j.chemgeo.2021.120403

Egan, H., Jarvinen, R., Ma, Y., & Brain, D. (2019). Planetary magnetic field control of ion escape from weakly magnetized planets. *Monthly Notices of the Royal Astronomical Society*, *488*(2), 2108–2120. https://doi.org/10.1093/mnras/stz1819

Ehlmann, B., Anderson, F., Andrews-Hanna, J., Catling, D., Christensen, P., Cohen, B., et al. (2016). The sustainability of habitability on terrestrial planets: Insights, questions, and needed measurements from Mars for understanding the evolution of Earth-like worlds. *Journal of Geophysical Research: Planets*, *121*(10), 1927–1961. https://doi.org/10.1002/2016je005134

Ehlmann, B. L., Mustard, J. F., Fassett, C. I., Schon, S. C., HeadIII, J. W., Des Marais, D. J., et al. (2008). Clay minerals in delta deposits and organic preservation potential on Mars. *Nature Geoscience*, *1*(6), 355–358. https://doi.org/10.1038/ngeo207

Ehlmann, B. L., Mustard, J. F., Murchie, S. L., Poulet, F., Bishop, J. L., Brown, A. J., et al. (2008). Orbital identification of carbonate-bearing rocks on Mars. *Science*, *322*(5909), 1828–1832. https://doi.org/10.1126/science.1164759

Eigenbrode, J. L., Summons, R. E., Steele, A., Freissinet, C., Millan, M., Navarro-González, R., et al. (2018). Organic matter preserved in 3-billion-year-old mudstones at Gale crater, Mars. *Science*, *360*(6393), 1096–1101. https://doi.org/10.1126/science.aas9185

Eiler, J. M., Valley, J. W., Graham, C. M., & Fournelle, J. (2002). Two populations of carbonate in ALH84001: Geochemical evidence for discrimination and genesis. *Geochimica et Cosmochimica Acta*, *66*(7), 1285–1303. https://doi.org/10.1016/s0016-7037(01)00847-x

Farley, K., Stack, K., Shuster, D., Horgan, B., Hurowitz, J., Tarnas, J., et al. (2022). Aqueously altered igneous rocks sampled on the floor of Jezero crater, Mars. *Science*, *377*(6614), eabo2196. https://doi.org/10.1126/science.abo2196

Farley, K. A., Williford, K. H., Stack, K. M., Bhartia, R., Chen, A., de la Torre, M., et al. (2020). Mars 2020 mission overview. *Space Science Reviews*, *216*(8), 1–41. https://doi.org/10.1007/s11214-020-00762-y

Fassett, C. I., & Head, J. W. (2011). Sequence and timing of conditions on early Mars. *Icarus*, *211*(2), 1204–1214. https://doi.org/10.1016/j.icarus.2010.11.014

Fassett, C. I., & Head III, J. W. (2005). Fluvial sedimentary deposits on Mars: Ancient deltas in a crater lake in the Nili Fossae region. *Geophysical Research Letters*, *32*(14), L14201. https://doi.org/10.1029/2005GL023456

Fassett, C. I., & Head III, J. W. (2008). The timing of Martian valley network activity: Constraints from buffered crater counting. *Icarus*, *195*(1), 61–89. https://doi.org/10.1016/j.icarus.2007.12.009

Feldman, W., Mellon, M., Maurice, S., Prettyman, T., Carey, J., Vaniman, D., et al. (2004). Hydrated states of $MgSO_4$ at equatorial latitudes on Mars. *Geophysical Research Letters*, *31*(16), L16702. https://doi.org/10.1029/2004GL020181

Feldman, W., Prettyman, T., Maurice, S., Plaut, J., Bish, D., Vaniman, D., et al. (2004). Global distribution of near-surface hydrogen on Mars. *Journal of Geophysical Research*, *109*(E9), E09006. https://doi.org/10.1029/2003JE002160

Fox, A., Eigenbrode, J., & Freeman, K. (2019). Radiolysis of macromolecular organic material in Mars-relevant mineral matrices. *Journal of Geophysical Research: Planets*, *124*(12), 3257–3266. https://doi.org/10.1029/2019je006072

François, P., Szopa, C., Buch, A., Coll, P., McAdam, A. C., Mahaffy, P. R., et al. (2016). Magnesium sulfate as a key mineral for the detection of organic molecules on Mars using pyrolysis. *Journal of Geophysical Research: Planets*, *121*(1), 61–74. https://doi.org/10.1002/2015je004884

Franz, H., Mahaffy, P., Webster, C., Flesch, G., Raaen, E., Freissinet, C., et al. (2020). Indigenous and exogenous organics and surface–atmosphere cycling inferred from carbon and oxygen isotopes at Gale crater. *Nature Astronomy*, *4*(5), 526–532. https://doi.org/10.1038/s41550-019-0990-x

Gaft, M., Reisfeld, R., & Panczer, G. (2015). *Modern luminescence spectroscopy of minerals and materials*. Springer International Publishing.

Glavin, D. P., Bada, J. L., Brinton, K. L., & McDonald, G. D. (1999). Amino acids in the Martian meteorite Nakhla. *Proceedings of the National Academy of Sciences*, *96*(16), 8835–8838. https://doi.org/10.1073/pnas.96.16.8835

Gosse, J. C., & Phillips, F. M. (2001). Terrestrial in situ cosmogenic nuclides: Theory and application. *Quaternary Science Reviews*, *20*(14), 1475–1560. https://doi.org/10.1016/S0277-3791(00)00171-2

Goudge, T. A., Mustard, J. F., Head, J. W., Fassett, C. I., & Wiseman, S. M. (2015). Assessing the mineralogy of the watershed and fan deposits of the Jezero crater paleolake system, Mars. *Journal of Geophysical Research: Planets*, *120*(4), 775–808. https://doi.org/10.1002/2014je004782

Graham, J. W. (1949). The stability and significance of magnetism in sedimentary rocks. *Journal of Geophysical Research*, *54*(2), 131–167. https://doi.org/10.1029/JZ054i002p00131

Grant, J. A., Golombek, M. P., Wilson, S. A., Farley, K. A., Williford, K. H., & Chen, A. (2018). The science process for selecting the landing site for the 2020 Mars rover. *Planetary and Space Science*, *164*, 106–126. https://doi.org/10.1016/j.pss.2018.07.001

Green, N. J., Xu, J., & Sutherland, J. D. (2021). Illuminating life's origins: UV photochemistry in abiotic synthesis of biomolecules. *Journal of the American Chemical Society*, *143*(19), 7219–7236. https://doi.org/10.1021/jacs.1c01839

Greenwood, J. P., Itoh, S., Sakamoto, N., Vicenzi, E. P., & Yurimoto, H. (2008). Hydrogen isotope evidence for loss of water from Mars through time. *Geophysical Research Letters*, *35*(5), L05203. https://doi.org/10.1029/2007GL032721

Gregory, D. D., Large, R. R., Halpin, J. A., Baturina, E. L., Lyons, T. W., Wu, S., et al. (2015). Trace element content of sedimentary pyrite in black shales. *Economic Geology*, *110*(6), 1389–1410. https://doi.org/10.2113/econgeo.110.6.1389

Grotzinger, J. P., Arvidson, R., Bell Iii, J., Calvin, W., Clark, B., Fike, D., et al. (2005). Stratigraphy and sedimentology of a dry to wet eolian depositional system, Burns formation, Meridiani Planum, Mars. *Earth and Planetary Science Letters*, *240*(1), 11–72. https://doi.org/10.1016/j.epsl.2005.09.039

Grotzinger, J. P., Sumner, D. Y., Kah, L., Stack, K., Gupta, S., Edgar, L., et al. (2014). A habitable fluvio-lacustrine environment at Yellowknife Bay, Gale Crater, Mars. *Science*, *343*(6169), 1242777. https://doi.org/10.1126/science.1242777

Halevy, I., Fischer, W. W., & Eiler, J. M. (2011). Carbonates in the Martian meteorite Allan Hills 84001 formed at 18±4°C in a near-surface aqueous environment. *Proceedings of the National Academy of Sciences*, *108*(41), 16895–16899. https://doi.org/10.1073/pnas.1109444108

Hassler, D. M., Zeitlin, C., Wimmer-Schweingruber, R. F., Ehresmann, B., Rafkin, S., Eigenbrode, J. L., et al. (2014). Mars' surface radiation environment measured with the Mars Science Laboratory's Curiosity rover. *Science*, *343*(6169), 1244797. https://doi.org/10.1126/science.1244797

Hausrath, E. M., Sullivan, R., Goreva, Y., Zorzano, M. P., Cardarelli, E., et al. (2023). The first regolith samples on Mars. *Paper presented at the 54th Lunar and Planetary Science Conference, The Woodlands, TX*.

Henneke, J., Pedersen, D. A. K., Liu, Y., Jörgensen, J., Denver, T., Rice, M., et al. (2023). A radiometric correction method and performance characteristics for PIXL's multispectral analysis using LED. *Space Science Reviews*, *219*(8), 68. https://doi.org/10.1007/s11214-023-01014-5

Hickman-Lewis, K., Cavalazzi, B., Foucher, F., & Westall, F. (2018). Most ancient evidence for life in the Barberton greenstone belt: Microbial mats and biofabrics of the~ 3.47 Ga Middle Marker horizon. *Precambrian Research*, *312*, 45–67. https://doi.org/10.1016/j.precamres.2018.04.007

Hickman-Lewis, K., Garwood, R. J., Brasier, M. D., Goral, T., Jiang, H., McLoughlin, N., & Wacey, D. (2016). Carbonaceous microstructures from sedimentary laminated chert within the 3.46 Ga Apex Basalt, Chinaman Creek locality, Pilbara, western Australia. *Precambrian Research*, *278*, 161–178. https://doi.org/10.1016/j.precamres.2016.03.013

Hickman-Lewis, K., Westall, F., & Cavalazzi, B. (2019). Chapter 42 - Traces of early life from the Barberton greenstone belt, South Africa. In M. J. Van Kranendonk, V. C. Bennett, & J. E. Hoffmann (Eds.), *Earth's oldest rocks* (2nd ed., pp. 1029–1058). Elsevier.

Hofmann, A. (2005). The geochemistry of sedimentary rocks from the Fig Tree Group, Barberton greenstone belt: Implications for tectonic, hydrothermal and surface processes during mid-Archaean times. *Precambrian Research*, *143*(1–4), 23–49. https://doi.org/10.1016/j.precamres.2005.09.005

Holm-Alwmark, S., Kinch, K., Hansen, M., Shahrzad, S., Svennevig, K., Abbey, W., et al. (2021). Stratigraphic relationships in Jezero crater, Mars: Constraints on the timing of fluvial-lacustrine activity from orbital observations. *Journal of Geophysical Research: Planets*, *126*(7), e2021JE006840. https://doi.org/10.1029/2021je006840

Homann, M. (2019). Earliest life on earth: Evidence from the Barberton greenstone belt, South Africa. *Earth-Science Reviews*, *196*, 102888. https://doi.org/10.1016/j.earscirev.2019.102888

Horgan, B. H., Anderson, R. B., Dromart, G., Amador, E. S., & Rice, M. S. (2020). The mineral diversity of Jezero crater: Evidence for possible lacustrine carbonates on Mars. *Icarus*, *339*, 113526. https://doi.org/10.1016/j.icarus.2019.113526

House, C. H., Wong, G. M., Webster, C. R., Flesch, G. J., Franz, H. B., Stern, J. C., et al. (2022). Depleted carbon isotope compositions observed at Gale crater, Mars. *Proceedings of the National Academy of Sciences, 119, e2115651119*.

Hurowitz, J. A., Tice, M. M., Allwood, A. C., Cable, M. L., Bosak, T., Broz, A., et al. (2023). The petrogenetic history of the Jezero crater delta front from microscale observations by the Mars 2020 PIXL instrument. *Paper presented at the 54th Lunar and Planetary Science Conference, The Woodlands, TX*.

Karamian, E., & Sharifnia, S. (2016). On the general mechanism of photocatalytic reduction of CO_2. *Journal of CO2 Utilization*, *16*, 194–203. https://doi.org/10.1016/j.jcou.2016.07.004

Karunatillake, S., Wray, J. J., Gasnault, O., McLennan, S. M., Rogers, A. D., Squyres, S. W., et al. (2014). Sulfates hydrating bulk soil in the Martian low and middle latitudes. *Geophysical Research Letters*, *41*(22), 7987–7996. https://doi.org/10.1002/2014gl061136

King, P. L., & McLennan, S. M. (2010). Sulfur on Mars. *Elements*, *6*(2), 107–112. https://doi.org/10.2113/gselements.6.2.107

Lagaly, G., Ogawa, M., & Dékány, I. (2006). Chapter 7.3 Clay mineral organic interactions. In F. Bergaya, B. K. G. Theng, & G. Lagaly (Eds.), *Developments in clay science* (Vol. 1, pp. 309–377). Elsevier. https://doi.org/10.1016/s1572-4352(05)01010-x

Lazar, O. R., Bohacs, K. M., Macquaker, J. H., Schieber, J., & Demko, T. M. (2015). Capturing key attributes of fine-grained sedimentary rocks in outcrops, cores, and thin sections: Nomenclature and description guidelines. *Journal of Sedimentary Research*, *85*(3), 230–246. https://doi.org/10.2110/jsr.2015.11

Leshin, L. A. (2000). Insights into martian water reservoirs from analyses of martian meteorite QUE94201. *Geophysical Research Letters*, *27*(14), 2017–2020. https://doi.org/10.1029/1999gl008455

Leshin, L. A., Epstein, S., & Stolper, E. M. (1996). Hydrogen isotope geochemistry of SNC meteorites. *Geochimica et Cosmochimica Acta*, *60*(14), 2635–2650. https://doi.org/10.1016/0016-7037(96)00122-6

Lopez-Reyes, G., Nachon, M., Veneranda, M., Beyssac, O., Madariaga, J. M., Manrique, J. A., & the SuperCam team. (2023). Anhydrite detections by Raman spectroscopy with SuperCam at the Jezero delta, Mars. *Paper presented at the 54th Lunar and Planetary Science Conference, The Woodlands, TX*.

Macey, M. C., Ramkissoon, N. K., Cogliati, S., Toubes-Rodrigo, M., Stephens, B. P., Kucukkilic-Stephens, E., et al. (2023). Habitability and biosignature formation in simulated Martian aqueous environments. *Astrobiology*, *23*(2), 144–154. https://doi.org/10.1089/ast.2021.0197

Mangold, N., Dromart, G., Ansan, V., Salese, F., Kleinhans, M. G., Massé, M., et al. (2020). Fluvial regimes, morphometry, and age of Jezero crater paleolake inlet valleys and their exobiological significance for the 2020 Rover Mission Landing Site. *Astrobiology*, *20*(8), 994–1013. https://doi.org/10.1089/ast.2019.2132

Mangold, N., Gupta, S., Gasnault, O., Dromart, G., Tarnas, J. D., Sholes, S. F., et al. (2021). Perseverance rover finds evidence for ancient delta and flood deposits at Jezero crater, Mars. *Science*, *374*(6568), 711–717. https://doi.org/10.1126/science.abl4051

Mariotti, G., Perron, J., & Bosak, T. (2014). Feedbacks between flow, sediment motion and microbial growth on sand bars initiate and shape elongated stromatolite mounds. *Earth and Planetary Science Letters*, *397*, 93–100. https://doi.org/10.1016/j.epsl.2014.04.036

Martin, P. E., Farley, K. A., Douglas Archer Jr, P., Hogancamp, J. V., Siebach, K. L., Grotzinger, J. P., & McLennan, S. M. (2020). Reevaluation of perchlorate in Gale crater rocks suggests geologically recent perchlorate addition. *Journal of Geophysical Research: Planets*, *125*(2), e2019JE006156. https://doi.org/10.1029/2019je006156

Maurice, S., Feldman, W., Diez, B., Gasnault, O., Lawrence, D. J., Pathare, A., & Prettyman, T. (2011). Mars Odyssey neutron data: 1. Data processing and models of water-equivalent-hydrogen distribution. *Journal of Geophysical Research*, *116*, E11. https://doi.org/10.1029/2011je003810

Maurice, S., Wiens, R. C., Bernardi, P., Caïs, P., Robinson, S., Nelson, T., et al. (2021). The SuperCam instrument suite on the Mars 2020 rover: Science objectives and mast-unit description. *Space Science Reviews*, *217*(3), 1–108. https://doi.org/10.1007/s11214-021-00807-w

McLennan, S. M., Bell, J., III, Calvin, W., Christensen, P., Clark, B., de Souza, P., et al. (2005). Provenance and diagenesis of the evaporite-bearing Burns formation, Meridiani Planum, Mars. *Earth and Planetary Science Letters*, *240*(1), 95–121. https://doi.org/10.1016/j.epsl.2005.09.041

McLennan, S. M., Grotzinger, J. P., Hurowitz, J. A., & Tosca, N. J. (2019). The sedimentary cycle on Early Mars. *Annual Review of Earth and Planetary Sciences*, *47*(1), 91–118. https://doi.org/10.1146/annurev-earth-053018-060332

McMahon, S., Bosak, T., Grotzinger, J., Milliken, R., Summons, R., Daye, M., et al. (2018). A field guide to finding fossils on Mars. *Journal of Geophysical Research: Planets*, *123*(5), 1012–1040. https://doi.org/10.1029/2017JE005478

Menor-Salván, C., & Marín-Yaseli, M. R. (2012). Prebiotic chemistry in eutectic solutions at the water–ice matrix. *Chemical Society Reviews*, *41*(16), 5404–5415. https://doi.org/10.1039/C2CS35060B

Millan, M., Teinturier, S., Malespin, C., Bonnet, J., Buch, A., Dworkin, J. P., et al. (2022). Organic molecules revealed in Mars's Bagnold Dunes by Curiosity's derivatization experiment. *Nature Astronomy*, *6*(1), 129–140. https://doi.org/10.1038/s41550-021-01507-9

Millan, M., Williams, A. J., Mcadam, A. C., Eigenbrode, J. L., Steele, A., Freissinet, C., et al. (2022). Sedimentary organics in Glen Torridon, Gale Crater, Mars: Results from the SAM instrument suite and supporting laboratory analyses. *Journal of Geophysical Research: Planets*, *127*(11), e2021JE007107. https://doi.org/10.1029/2021je007107

Minitti, M., Kennedy, M., Edgett, K., Beegle, L., Asher, S., Abbey, W., et al. (2021). The Mars 2020 Watson imaging subsystem of the Sherloc investigation and anticipated early results. *Paper presented at the 53rd Lunar and Planetary Science Conference, The Woodlands, TX*.

Mittelholz, A., Morschhauser, A., Johnson, C. L., Langlais, B., Lillis, R. J., Vervelidou, F., & Weiss, B. P. (2018). The Mars 2020 candidate landing sites: A magnetic field perspective. *Earth and Space Science*, *5*(9), 410–424. https://doi.org/10.1029/2018ea000420

Mittlefehldt, D. W. (1994). ALH84001, a cumulate orthopyroxenite member of the Martian meteorite clan. *Meteoritics*, *29*(6), 214–221. https://doi.org/10.1111/j.1945-5100.1994.tb01106.x

Moeller, R. C., Jandura, L., Rosette, K., Robinson, M., Samuels, J., Silverman, M., et al. (2021). The sampling and caching Subsystem (SCS) for the scientific exploration of Jezero crater by the Mars 2020 Perseverance rover. *Space Science Reviews*, *217*, 1–43. https://doi.org/10.1007/s11214-020-00783-7

Mojarro, A., Buch, A., Dworkin, J. P., Eigenbrode, J. L., Fressinet, C., Glavin, D. P., et al. (2023). Murchison meteorite analysis using tetramethylammonium hydroxide (TMAH) thermochemolysis under simulated sample analysis at Mars (SAM) pyrolysis-gas chromatography-mass spectrometry conditions. *Journal of Geophysical Research: Planets*, *128*(11), e2023JE007968. https://doi.org/10.1029/2023je007968

Moore, K. R., Daye, M., Gong, J., Williford, K., Konhauser, K., & Bosak, T. (2023). A review of microbial-environmental interactions recorded in Proterozoic carbonate-hosted chert. *Geobiology*, *21*(1), 3–27. https://doi.org/10.1111/gbi.12527

Morris, R. V., Ruff, S. W., Gellert, R., Ming, D. W., Arvidson, R. E., Clark, B. C., et al. (2010). Identification of carbonate-rich outcrops on Mars by the Spirit rover. *Science*, *329*(5990), 421–424. https://doi.org/10.1126/science.1189667

Morrison, J., Brockwell, T., Merren, T., Fourel, F., & Phillips, A. M. (2001). On-line high-precision stable hydrogen isotopic analyses on nanoliter water samples. *Analytical Chemistry*, *73*(15), 3570–3575. https://doi.org/10.1021/ac001447t

Murchie, S. L., Mustard, J. F., Ehlmann, B. L., Milliken, R. E., Bishop, J. L., McKeown, N. K., et al. (2009). A synthesis of Martian aqueous mineralogy after 1 Mars year of observations from the Mars Reconnaissance Orbiter. *Journal of Geophysical Research*, *114*(E2), E00D06. https://doi.org/10.1029/2009je003342

Nachon, M., Lopez-Reyes, G., Meslin, P.-Y., Ollila, A., Mandon, L., & the SuperCam team. (2023). Light-toned veins and material in Jezero crater, Mars, as seen in-situ via NASA's Perseverance rover (Mars 2020 mission): Stratigraphic distribution and compositional results from the SuperCam instrument. *Paper presented at the 54th Lunar and Planetary Science Conference, The Woodlands, TX*.

National Academies of Sciences, Engineering, and Medicine. (2022). *Origins, Worlds, and life: A decadal strategy for planetary science and Astrobiology 2023-2032*. The National Academies Press. https://doi.org/10.17226/26522

National Research Council. (2011). *Vision and Voyages for planetary science in the decade 2013-2022*. The National Academies Press. https://doi.org/10.17226/13117

Niles, P., Leshin, L., & Guan, Y. (2005). Microscale carbon isotope variability in ALH84001 carbonates and a discussion of possible formation environments. *Geochimica et Cosmochimica Acta*, *69*(11), 2931–2944. https://doi.org/10.1016/j.gca.2004.12.012

Nutman, A. P., Bennett, V. C., Friend, C. R., Van Kranendonk, M. J., & Chivas, A. R. (2016). Rapid emergence of life shown by discovery of 3,700-million-year-old microbial structures. *Nature*, *537*(7621), 535–538. https://doi.org/10.1038/nature19355

Ono, S. (2017). Photochemistry of sulfur dioxide and the origin of mass-independent isotope fractionation in Earth's atmosphere. *Annual Review of Earth and Planetary Sciences*, *45*(1), 301–329. https://doi.org/10.1146/annurev-earth-060115-012324

Ono, S., Beukes, N. J., & Rumble, D. (2009). Origin of two distinct multiple-sulfur isotope compositions of pyrite in the 2.5 Ga Klein Naute formation, Griqualand west basin, South Africa. *Precambrian Research*, *169*(1–4), 48–57. https://doi.org/10.1016/j.precamres.2008.10.012

Patel, B. H., Percivalle, C., Ritson, D. J., Duffy, C. D., & Sutherland, J. D. (2015). Common origins of RNA, protein and lipid precursors in a cyanosulfidic protometabolism. *Nature Chemistry*, *7*(4), 301–307. https://doi.org/10.1038/nchem.2202

Pavlov, A., Vasilyev, G., Ostryakov, V., Pavlov, A., & Mahaffy, P. (2012). Degradation of the organic molecules in the shallow subsurface of Mars due to irradiation by cosmic rays. *Geophysical Research Letters*, *39*(13), L13202. https://doi.org/10.1029/2012gl052166

Petsch, S. T., Berner, R. A., & Eglinton, T. I. (2000). A field study of the chemical weathering of ancient sedimentary organic matter. *Organic Geochemistry*, *31*(5), 475–487. https://doi.org/10.1016/s0146-6380(00)00014-0

Poulet, F., Bibring, J.-P., Mustard, J., Gendrin, A., Mangold, N., Langevin, Y., et al. (2005). Phyllosilicates on Mars and implications for early Martian climate. *Nature*, *438*(7068), 623–627. https://doi.org/10.1038/nature04274

Powner, M. W., Gerland, B., & Sutherland, J. D. (2009). Synthesis of activated pyrimidine ribonucleotides in prebiotically plausible conditions. *Nature*, *459*(7244), 239–242. https://doi.org/10.1038/nature08013

Quantin-Nataf, C., Alwmark, S., Calef, F., Lasue, J., Kinch, K., Stack, K., et al. (2023). The complex exhumation history of Jezero crater floor unit and its implication for Mars sample return. *Journal of Geophysical Research: Planets*, *128*(6), e2022JE007628. https://doi.org/10.1029/2022je007628

Razzell Hollis, J., Abbey, W., Beegle, L. W., Bhartia, R., Ehlmann, B. L., Miura, J., et al. (2021). A deep-ultraviolet Raman and fluorescence spectral library of 62 minerals for the SHERLOC instrument onboard Mars 2020. *Planetary and Space Science*, *209*, 105356. https://doi.org/10.1016/j.pss.2021.105356

Razzell Hollis, J., Moore, K. R., Sharma, S., Beegle, L., Grotzinger, J. P., Allwood, A., et al. (2022). The power of paired proximity science observations: Co-Located data from SHERLOC and PIXL on Mars. *Icarus*, *387*, 115179. https://doi.org/10.1016/j.icarus.2022.115179

Rosing, M. T. (1999). ^{13}C-depleted carbon microparticles in> 3700-Ma sea-floor sedimentary rocks from West Greenland. *Science*, *283*(5402), 674–676. https://doi.org/10.1126/science.283.5402.674

Ross, D. S., & Deamer, D. (2016). Dry/wet cycling and the thermodynamics and kinetics of prebiotic polymer synthesis. *Life*, *6*(3), 28. https://doi.org/10.3390/life6030028

Scheller, E., Ehlmann, B., Hu, R., Adams, D., & Yung, Y. (2021). Long-term drying of Mars by sequestration of ocean-scale volumes of water in the crust. *Science*, *372*(6537), 56–62. https://doi.org/10.1126/science.abc7717

Scheller, E. L., Bosak, T., McCubbin, F. M., Williford, K., Siljestrom, S., Jakubek, R. S., et al. (2024). Inorganic interpretation of luminescent materials in Jezero crater's floor and delta on Mars. *Paper presented at the 55th Lunar and Planetary Science Conference, The Woodlands, TX*.

Scheller, E. L., Razzell Hollis, J., Cardarelli, E. L., Steele, A., Beegle, L. W., Bhartia, R., et al. (2022). Aqueous alteration processes in Jezero crater, Mars—Implications for organic geochemistry. *Science*, *378*(6624), 1105–1110. https://doi.org/10.1126/science.abo5204

Schon, S. C., Head, J. W., & Fassett, C. I. (2012). An overfilled lacustrine system and progradational delta in Jezero crater, Mars: Implications for Noachian climate. *Planetary and Space Science*, *67*(1), 28–45. https://doi.org/10.1016/j.pss.2012.02.003

Sharma, S., Roppel, R. D., Murphy, A. E., Beegle, L. W., Bhartia, R., Steele, A., et al. (2023). Diverse organic-mineral associations in Jezero crater, Mars. *Nature*, *619*(7971), 1–9. https://doi.org/10.1038/s41586-023-06143-z

Shkolyar, S., Lalla, E., Konstantindis, M., Cote, K., Daly, M., & Steele, A. (2021). Detecting Ce^{3+} as a biosignature mimicker using UV time-resolved laser-induced fluorescence and Raman spectroscopy: Implications for planetary missions. *Icarus*, *354*, 114093. https://doi.org/10.1016/j.icarus.2020.114093

Shuster, D. L., Farley, K. A., Bosak, T., Czaja, A. D., Hausrath, E. M., Mayhew, L. M., & and the Mars 2020 team. (2023). [Initial Report] Mars 2020 initial reports volume 2. Retrieved from https://pds-geosciences.wustl.edu/m2020/urn-nasa-pds-mars2020_sample_dossier/initial_reports/initial_reports_volume2.pdf

Sim, M. S., Bosak, T., & Ono, S. (2011). Large sulfur isotope fractionation does not require disproportionation. *Science*, *333*(6038), 74–77. https://doi.org/10.1126/science.1205103

Simon, J., Hickman-Lewis, K., Cohen, B., Mayhew, L., Shuster, D., Debaille, V., et al. (2023). Samples collected from the floor of Jezero crater with the Mars 2020 Perseverance rover. *Journal of Geophysical Research: Planets*, *128*(6), e2022JE007474. https://doi.org/10.1029/2022je007474

Squyres, S. W., Grotzinger, J. P., Arvidson, R. E., Bell III, J. F., Calvin, W., Christensen, P. R., et al. (2004). In situ evidence for an ancient aqueous environment at Meridiani Planum, Mars. *Science*, *306*(5702), 1709–1714. https://doi.org/10.1126/science.1104559

Stack, K. M., Ives, L., Gupta, S., Lamb, M., Tebolt, M., Caravaca, G., et al. (2024). Sedimentology and stratigraphy of the Shenandoah formation, Western sediment fan, Jezero crater, Mars. *Journal of Geophysical Research: Planets*, *129*(2), e2023JE008187. https://doi.org/10.1029/2023je008187

Stack, K. M., Williams, N. R., Calef, F., Sun, V. Z., Williford, K. H., Farley, K. A., et al. (2020). Photogeologic map of the Perseverance rover field site in Jezero crater constructed by the Mars 2020 Science Team. *Space Science Reviews*, *216*(8), 1–47. https://doi.org/10.1007/s11214-020-00739-x

Steele, A., McCubbin, F. M., & Fries, M. D. (2016). The provenance, formation, and implications of reduced carbon phases in Martian meteorites. *Meteoritics & Planetary Sciences*, *51*(11), 2203–2225. https://doi.org/10.1111/maps.12670

Stern, J. C., Malespin, C. A., Eigenbrode, J. L., Webster, C. R., Flesch, G., Franz, H. B., et al. (2022). Organic carbon concentrations in 3.5-billion-year-old lacustrine mudstones of Mars. *Proceedings of the National Academy of Sciences* (Vol. 119, p. e2201139119).

Sugitani, K., Mimura, K., Nagaoka, T., Lepot, K., & Takeuchi, M. (2013). Microfossil assemblage from the 3400 Ma Strelley Pool formation in the Pilbara Craton, western Australia: Results form a new locality. *Precambrian Research*, *226*, 59–74. https://doi.org/10.1016/j.precamres.2012.11.005

Sumner, D. Y. (2004). Poor preservation potential of organics in Meridiani Planum hematite-bearing sedimentary rocks. *Journal of Geophysical Research*, *109*, E12. https://doi.org/10.1029/2004je002321

Sutter, B., Mcadam, A. C., Mahaffy, P. R., Ming, D. W., Edgett, K. S., Rampe, E. B., et al. (2017). Evolved gas analyses of sedimentary rocks and eolian sediment in Gale Crater, Mars: Results of the Curiosity rover's sample analysis at Mars instrument from Yellowknife Bay to the Namib Dune. *Journal of Geophysical Research: Planets*, *122*(12), 2574–2609. https://doi.org/10.1002/2016je005225

Szopa, C., Freissinet, C., Glavin, D. P., Millan, M., Buch, A., Franz, H. B., et al. (2020). First detections of dichlorobenzene isomers and trichloromethylpropane from organic matter indigenous to Mars mudstone in Gale Crater, Mars: Results from the sample analysis at Mars instrument onboard the Curiosity rover. *Astrobiology*, *20*(2), 292–306. https://doi.org/10.1089/ast.2018.1908

Tate, C. D. (2023a). [3D visualization] M2020 ZCAM – Amalik and Enchanted Lake, sol 569. *Sketchfab*. Retrieved from https://sketchfab.com/3d-models/m2020-watson-novarupta-abrasion-sol-568-be98ff3369e145899267ac71cece294a

Tate, C. D. (2023b). [3D visualization] M2020 ZCAM – Amalik workspace, sol 590. *Sketchfab*. Retrieved from https://sketchfab.com/3d-models/m2020-zcam-amalik-after-sampling-sol-590-ae70df2eda8e4d5589269b76e3aea36b

Tate, C. D. (2023c). [3D visualization] M2020 ZCAM – Novarupta abrasion patch, sol 568. *Sketchfab*. Retrieved from https://sketchfab.com/3d-models/m2020-watson-novarupta-abrasion-sol-568-be98ff3369e145899267ac71cece294a

Tate, C. D. (2023d). [3D visualization] M2020 ZCAM – Wildcat Ridge workspace, sol 502. *Sketchfab*. Retrieved from https://sketchfab.com/3d-models/m2020-zcam-wildcat-ridge-sol-502-aa7a278ba53e428ca8f7103eff79987a

Tate, C. D. (2023e). [3D visualization] M2020 ZCAM – Berry Hollow abrasion patch. *Sketchfab*. Retrieved from https://sketchfab.com/3d-models/mars2020-berry-hollow-abrasion-focused-view-d5e24e8c7bde45f8bb43f9a70ecd2b21

Tate, C. D. (2023f). [3D visualization] M2020 ZCAM – Hidden Harbor area, sol 609. *Sketchfab*. Retrieved from https://sketchfab.com/3d-models/m2020-zcam-hidden-harbor-sol-609-62be9a238f8e4b748359a561c58dd83a

Tate, C. D. (2023g). [3D visualization] M2020 ZCAM – Uganik Island abrasion, sol 612. *Sketchfab*. Retrieved from https://sketchfab.com/3d-models/m2020-watson-uganik-island-sol-612-a5cb734f16684ed09b90a9d1c926ddd4

Tate, C. D. (2023h). [3D visualization] M2020 ZCAM – Skinner Ridge area. *Sketchfab*. Retrieved from https://sketchfab.com/3d-models/m2020-zcam-oventop-mountain-sol-477-21ddf211a0a84c3f8d563a3d5f9cd4e3

Tate, C. D. (2023i). [3D visualization] M2020 ZCAM – Thornton Gap abrasion, sol 482. *Sketchfab*. Retrieved from https://sketchfab.com/3d-models/mars2020-thornton-gap-abrasion-sol-482-b188ac8ab373426694ddd65a4698d388

Thiemens, M. H., Savarino, J., Farquhar, J., & Bao, H. (2001). Mass-independent isotopic compositions in terrestrial and extraterrestrial solids and their applications. *Accounts of Chemical Research*, *34*(8), 645–652. https://doi.org/10.1021/ar960224f

Tice, M. M., & Lowe, D. R. (2004). Photosynthetic microbial mats in the 3,416-Myr-old ocean. *Nature*, *431*(7008), 549–552. https://doi.org/10.1038/nature02888

Tosca, N. J., Knoll, A. H., & McLennan, S. M. (2008). Water activity and the challenge for life on early Mars. *Science*, *320*(5880), 1204–1207. https://doi.org/10.1126/science.1155432

Trojanowicz, M. (2020). Removal of persistent organic pollutants (POPs) from waters and wastewaters by the use of ionizing radiation. *Science of the Total Environment*, *718*, 134425. https://doi.org/10.1016/j.scitotenv.2019.134425

Ueno, Y., Ono, S., Rumble, D., & Maruyama, S. (2008). Quadruple sulfur isotope analysis of ca. 3.5 Ga Dresser Formation: New evidence for microbial sulfate reduction in the early Archean. *Geochimica et Cosmochimica Acta*, *72*(23), 5675–5691. https://doi.org/10.1016/j.gca.2008.08.026

Usui, T., Alexander, C. M. D., Wang, J., Simon, J. I., & Jones, J. H. (2012). Origin of water and mantle–crust interactions on Mars inferred from hydrogen isotopes and volatile element abundances of olivine-hosted melt inclusions of primitive shergottites. *Earth and Planetary Science Letters*, *357*, 119–129. https://doi.org/10.1016/j.epsl.2012.09.008

Usui, T., Alexander, C. M. O. D., Wang, J., Simon, J. I., & Jones, J. H. (2015). Meteoritic evidence for a previously unrecognized hydrogen reservoir on Mars. *Earth and Planetary Science Letters*, *410*, 140–151. https://doi.org/10.1016/j.epsl.2014.11.022

Valley, J. W., Eiler, J. M., Graham, C. M., Gibson, E. K., Romanek, C. S., & Stolper, E. M. (1997). Low-temperature carbonate concretions in the Martian meteorite ALH84001: Evidence from stable isotopes and mineralogy. *Science*, *275*(5306), 1633–1638. https://doi.org/10.1126/science.275.5306.1633

Vaniman, D. T., Bish, D. L., Chipera, D. J., Fialips, C. I., William Carey, J., & Feldman, W. C. (2004). Magnesium sulphate salts and the history of water on Mars. *Nature*, *431*(7009), 663–665. https://doi.org/10.1038/nature02973

Vaniman, D. T., Martinez, G. M., Rampe, E. B., Bristow, T. F., Blake, D. F., Yen, A. S., et al. (2018). Gypsum, bassanite, and anhydrite at Gale crater, Mars. *American Mineralogist*, *103*(7), 1011–1020. https://doi.org/10.2138/am-2018-6346

van Zuilen, M. A., Chaussidon, M., Rollion-Bard, C., & Marty, B. (2007). Carbonaceous cherts of the Barberton Greenstone Belt, South Africa: Isotopic, chemical and structural characteristics of individual microstructures. *Geochimica et Cosmochimica Acta*, *71*(3), 655–669. https://doi.org/10.1016/j.gca.2006.09.029

Velbel, M. A., Cockell, C. S., Glavin, D. P., Marty, B., Regberg, A. B., Smith, A. L., et al. (2021). Planning implications related to sterilization-sensitive science investigations associated with Mars Sample Return (MSR). *Astrobiology*, *22*(S1), S-112. https://doi.org/10.1089/ast.2021.0113

Walsh, M. M., & Lowe, D. R. (1999). *Modes of accumulation of carbonaceous matter in the early Archean: A petrographic and geochemical study of the carbonaceous cherts of the Swaziland supergroup* (pp. 115–132). Special Papers-Geological Society of America.

Wang, A., Freeman, J. J., & Jolliff, B. L. (2009). Phase transition pathways of the hydrates of magnesium sulfate in the temperature range 50°C to 5°C: Implication for sulfates on Mars. *Journal of Geophysical Research*, *114*(E4), E04010. https://doi.org/10.1029/2008JE003266

Wang, A., Jolliff, B. L., Liu, Y., & Connor, K. (2016). Setting constraints on the nature and origin of the two major hydrous sulfates on Mars: Monohydrated and polyhydrated sulfates. *Journal of Geophysical Research: Planets*, *121*(4), 678–694. https://doi.org/10.1002/2015je004889

Weiss, B. P., Mansbach, E. N., Carsten, J. L., Kaplan, K. W., Maki, J. N., Wiens, R. C., et al. (2024). Oriented bedrock samples drilled by the Perseverance rover on Mars. *Earth and Space Science*, *11*(3), e2023EA003322. https://doi.org/10.1029/2023EA003322

Wentworth, C. K. (1922). A scale of grade and class terms for clastic sediments. *The Journal of Geology*, *30*(5), 377–392. https://doi.org/10.1086/622910

Werner, S. C. (2009). The global martian volcanic evolutionary history. *Icarus*, *201*(1), 44–68. https://doi.org/10.1016/j.icarus.2008.12.019

Westall, F., Campbell, K. A., Bréhéret, J. G., Foucher, F., Gautret, P., Hubert, A., et al. (2015). Archean (3.33 Ga) microbe-sediment systems were diverse and flourished in a hydrothermal context. *Geology*, *43*(7), 615–618. https://doi.org/10.1130/g36646.1

Whittig, L. D., Deyo, A. E., & Tanji, K. K. (1982). Evaporite mineral species in Mancos Shale and salt efflorescence, upper Colorado river basin. *Soil Science Society of America Journal*, *46*(3), 645–651. https://doi.org/10.2136/sssaj1982.03615995004600030039x

Wiens, R. C., Maurice, S., Robinson, S. H., Nelson, A. E., Cais, P., Bernardi, P., et al. (2021). The SuperCam instrument suite on the NASA Mars 2020 rover: Body unit and combined system tests. *Space Science Reviews*, *217*, 1–87. https://doi.org/10.1007/s11214-020-00777-5

Williams, J., Shearer, C., Sharp, Z., Burger, P., McCubbin, F., Santos, A., et al. (2016). The chlorine isotopic composition of Martian meteorites 1: Chlorine isotope composition of Martian mantle and crustal reservoirs and their interactions. *Meteoritics & Planetary Sciences*, *51*(11), 2092–2110. https://doi.org/10.1111/maps.12647

Williford, K. H., Farley, K. A., Stack, K. M., Allwood, A. C., Beaty, D., Beegle, L. W., et al. (2018). The NASA Mars 2020 rover mission and the search for extraterrestrial life. In *From habitability to life on Mars* (pp. 275–308). Elsevier.

Wilson, S., & Bish, D. L. (2012). Stability of Mg-sulfate minerals in the presence of smectites: Possible mineralogical controls on H_2O cycling and biomarker preservation on Mars. *Geochimica et Cosmochimica Acta*, *96*, 120–133. https://doi.org/10.1016/j.gca.2012.08.008

Wordsworth, R. D. (2016). The climate of early Mars. *Annual Review of Earth and Planetary Sciences*, *44*(1), 381–408. https://doi.org/10.1146/annurev-earth-060115-012355

Xu, J., Green, N. J., Russell, D. A., Liu, Z., & Sutherland, J. D. (2021). Prebiotic photochemical coproduction of purine ribo- and deoxy-ribonucleosides. *Journal of the American Chemical Society*, *143*(36), 14482–14486. https://doi.org/10.1021/jacs.1c07403

Zawaski, M. J., Kelly, N. M., Orlandini, O. F., Nichols, C. I., Allwood, A. C., & Mojzsis, S. J. (2020). Reappraisal of purported ca. 3.7 Ga stromatolites from the Isua Supracrustal Belt (West Greenland) from detailed chemical and structural analysis. *Earth and Planetary Science Letters*, *545*, 116409. https://doi.org/10.1016/j.epsl.2020.116409